EXTENSIVE AIR SHOWER EXPERIMENT AT KOLAR GOLD FIELDS

B.S.Acharya, S.Naranan, M.V.S.Rao, K.Sivaprasad,
B.V.Sreekantan and Srikantha Rao*

Tata Institute of Fundamental Research, Bombay 400005, India

Short Title : EAS EXPERIMENT AT KGF

ABSTRACT

An experiment to determine the nature of primary cosmic rays of energy > 10^{14} eV by studying high energy (> 220 GeV) muons and their correlations with other parameters of extensive air showers generated by them, was carried out at Kolar Gold Fields, India (atmospheric depth of 920 g cm^{-2}). Accurate estimate of shower parameters in showers of size as small as 10^4 particles was achieved by means of a closely packed array of large area detectors and by employing special methods of analysis. In this paper, the details of the array, the data recording system, the procedure of data analysis and error estimates are described.

* Now with the National Radio and Electronics Co. Ltd.,
Bombay 400 058, India.

To appear in Nuclear Instruments and Methods. 1988

1. Introduction

Study of ultra high energy (> 10^{14} eV) cosmic rays is important to gain knowledge regarding their origin as well as features of high energy interactions in an energy region inaccessible to accelerators. Investigation of Extensive Air Showers (EAS) generated by these cosmic rays is the only means of such a study at present because of their low fluxes. Features of EAS generally depend on the characteristics of high energy interactions as well as the nature of the primary particles. Of the various components of EAS, the high energy muon component carries information regarding these two aspects rather directly because of its origin in the first few generations of the EAS cascade [1]. We have earlier reported results on the gross features of high energy muons, in particular the variation of their number with shower size and their energy spectrum [2,3,4]. Interpretation of even such relatively direct information in terms of either the nature of the primary particles or features of high energy interactions uniquely, is difficult because of its sensitivity to both these aspects. The situation is even worse with regard to other EAS parameters e.g. hadrons, low energy muons etc. Special methods have to be developed in order to disentangle the effects due to these two aspects on EAS parameters ; e.g. study of correlations among properly chosen parameters.

We have shown [5,6] that a study of correlations between the density of low energy (>1 GeV) and high energy (>220 GeV) muons in showers of size ~ 10^4 particles (primary energy ~ 10^{14} eV) can yield unambiguous information regarding the nature of the primary particles. The negative correlation between the density of low energy muons at a fixed distance from the core and the number of high energy muons beyond a certain critical distance, in showers initiated by primaries of the same mass, can be exploited to discern between a primary cosmic ray composition that is 'mixed' and one that is dominated by a single species. Correlation between the age parameter of the shower and the distance at which the high energy muon is detected can also be similarly exploited.

An important feature of cosmic rays to be studied from the point of view of their origin is their energy spectrum. Direct measurements with detectors flown in satellites [7] have shown that the all particle integral energy spectrum (the spectrum of all species combined together) follows a power law with an exponent of -1.7 up to 10^{15} eV without any change in the exponent. Beyond this energy, the spectrum has been derived from EAS studies and the exponent in this energy region is about -2.1, suggesting that the primary energy spectrum becomes steeper at around a few times 10^{15} eV, thus forming the famous 'knee'. There are very few measurements from the EAS experiments below the knee to conclusively show that the knee is real. Models of the cosmic ray origin and propagation predict the primary cosmic ray composition to vary with energy in the neighbourhood of the knee, if it is real, in specific ways. Thus, it is essential to measure the the energy spectrum and the composition over a wide energy range including the knee.

We have carried out an experiment at Kolar Gold Fields (KGF, atmospheric depth : 920 g cm^{-2}) to elucidate on all these aspects. The experiment is designed to provide accurate information on the size spectrum (the dependence of the intensity of cosmic rays on size, the total number of particles contained in the showers generated by them) and the variation of the total number of muons of energy > 220 GeV with shower size over the size range 10^4 to 10^7, which covers the knee region, lateral distribution of these muons and their correlations with low energy muons and the age parameter in the lower energy region. The array consists of a large number of scintillation detectors to accurately measure the electron component, a

low energy (>1 GeV) muon detector and a neon flash tube telescope and scintillators located underground to measure muons of energy >220 GeV. Accurate estimate of shower parameters at sizes as small as 10^4 particles was achieved by deploying closely spaced large area detectors up to 20 m from the center of the array. A computerised recording system and an on-line calibration procedure was used to handle the large number of detectors. Particular attention was paid to the analysis of showers with small sizes to obtain their parameters accurately. In section 2, the design of the EAS array and the various detectors used to measure the different shower parameters are described. The various triggers used to collect the data, the recording system and the calibration of the detectors are described in section 3. The method of analysis used to estimate the shower parameters and their errors is described in section 4.

2. Experimental Set up

The extensive air shower array was specifically designed to detect and accurately measure showers of size as small as 10^4 particles as well as to collect enough number of showers of size 10^7 particles. This was achieved by placing a large number of closely packed large area detectors at the center of the array and extending the array up to 100 m from the center.

The experimental set up consisted of an array of 70 plastic scintillation detectors (density detectors) to detect the showers and to measure the shower particle densities, 5 fast liquid scintillation detectors to measure the arrival direction of the showers, a shielded plastic scintillation detector (low energy muon detector) of area 9 m^2 to measure muons of energy > 1 GeV and four plastic scintillators (high energy muon detectors) located 270 m underground, vertically below the EAS array to measure muons of energy > 220 GeV; two of the four scintillators underground were located inside and provide trigger for a Neon Flash Tube (NFT) telescope which locates the track of the muon. The plan of the array is shown in figure 1. The projection of the underground detectors on to the surface array plane is shown in figure 2, where the central part of the array is shown on an expanded scale. Underground detectors 1 and 2 are located inside the NFT telescope.

The inner 37 detectors were of 2.25 m^2 area each and were placed within 15 m from the center with hexagonal symmetry, the spacing between neighbouring detectors being 5 m. Six more detectors of the same area each were placed at 20 m from the center, one toward each side of the hexagon. This inner concentration of detectors made it possible to detect and locate cores with an accuracy of less than 1 m, even for showers with size as low as 10^4. The remaining detectors, each of area 1 m^2, were symmetrically placed on concentric circles of radii 40 m, 60 m and 100 m, with 12, 12 and 3 detectors respectively on each circle. These helped in the accurate determination of the lateral distribution of the showers as well as in eliminating the chance of large showers landing at large distances from the center, simulating small flat showers landing inside the array.

2.1 Density Detectors

Each density detector of area 2.25 m^2 consisted of nine (four in the case of 1 m^2 detectors) 50 cm x 50 cm x 5 cm plastic scintillator blocks viewed by a Dumont 6364 photomultiplier (cathode diameter 12.7 cm) from a height of 80 cm, all the elements held in a light tight pyramidal aluminum container. The walls and the base of the pyramid were coated inside with TiO_2 paint for good light reflection. The light emitted by the scintillator, when ionising particles passed through it, was thus diffused

before reaching the photocathode. Pulses from the photomultiplier were amplified by a high input impedance preamplifier [8] of gain 10 and transmitted to a central recording room by RG-11/U coaxial cable. Here the pulses were further amplified by a non-overloading amplifier by a factor of ~ 300, preserving the decay time of the pulses [8]. The decay time of the pulses from each detector was kept approximately at 5 μs by adjusting the anode resistance of the photomultiplier and the input capacitance of the preamplifier. The rise time of the pulses at the output of the 300 gain amplifiers varied from 100 ns to 500 ns, depending on the detector. The 300 gain amplifier was followed by a discriminator with an adjustable bias. As the decay time of the pulses was preserved, the width of the discriminator output was proportional to the logarithm of the height of the input pulse. Whenever certain trigger requirements were fulfilled (see section 3.1) the discriminator output was gated to a ramp followed by a stretching circuit where the ramp height was stored on a memory capacitor for later digitisation and recording. The discriminator bias was set such that single minimum ionising particles were detected with an efficiency of > 95%. The density range covered was from 0.5 m^{-2} to 500 m^{-2} in the case of 2.25 m^2 detectors and 1 m^{-2} to 1000 m^{-2} in the case of the 1 m^2 detectors. The calibration of the detectors and the relation of the recorded pulse width to the density of particles in the detector will be discussed in section 3.3.

In addition to the logarithmic output, a linear output after the gain of 300 was provided from each amplifier. This was to get the integral pulse height spectrum of cosmic rays to be used for monitoring and calibration of the detectors.

In order to select EAS, the preamplifier outputs from the innermost 37 detectors were also fed to another set of amplifiers, called 'selection' amplifiers, with a gain of 150, followed by a discriminator with adjustable bias. Two other sets of amplifier-discriminators for selecting showers in higher size ranges were also provided (see section 3.1).

2.2 Low Energy Muon detector

Four plastic scintillation detectors, each of area 2.25 m^2, and identical to the density detectors of the same area, were placed under a granite stack 2.55 m high. The shielding of the detectors was good up to ~ 60° from the vertical and corresponds to a penetration energy of 1 GeV for vertical muons. With a deBRity of 3.02 g cm^{-3}, Z/A of 0.5 and Z^2/A of 6.3, the shielding provided nearly 30 radiation lengths or 10 nuclear interaction lengths of matter for absorbing soft component and hadrons. Pulse processing and recording of information from these scintillators were identical to that of the density detectors.

2.3 Energy Flow Detectors

Two plastic scintillators of 1 m^2 area each were placed one below the other with 2.5 cm of lead between them. The relative pulse heights in the two detectors gave a measure of the energy flow in the soft component. Pulse processing, monitoring, calibration and data recording were identical to the density detectors. This pair of detectors was placed 6 m from the center of the array.

2.4 Fast Timing Detectors

These were 5 liquid scintillation detectors, each of area 1 m^2, and

viewed by a fast RCA 6810 (or Philips 56 AVP) photomultiplier. The liquid used was commercial grade Shellsol-A with paraterphenyl and POPOP as solutes. The detector had a cylindrical (pill box) geometry with a diameter of 1.15 m and a height of 30 cm. The efficiency for detecting minimum ionising particles was almost 100% even for edge traversals. One of the detectors, the central one, was placed 2 m to the North of the central density detector on the North-South axis, which was also the y-axis of the array coordinate system. The other four were placed on a circle of radius 15 m centered on the central timing detector, one each to the north, east, west and south of the center. The difference between the time of arrival of the pulses from the central detector and each of the other detectors was measured and stored on memory capacitors as a DC level to be digitised and recorded for each shower trigger. The timing accuracy of the electronic system alone was ~ 2 ns. Due to jitter in the photomultiplier and the spread in the path lengths traversed by the particles in the detector the ultimate resolution achieved was ~ 5 ns. With a base line of 15 m this gave an accuracy of ~ 5^{o} in the angle estimates for vertical showers.

2.5 High Energy Muon Detector

High energy muons were detected by 4 plastic scintillation detectors, each of area 1 m^2, placed underground 270 m vertically below the EAS array. They are similar to the 1 m^2 density detectors except that they are viewed by two Dumont 6364 photomultipliers each. The pulses from the photomultipliers were fed through an amplifier and discriminator whose bias and the high voltage for the photomultiplier tubes were adjusted so that minimum ionising particles were detected with an efficiency > 95% by each photomultiplier. At an ambient temperature of ~ 32^{o} C this lead to a large rate (~ a few thousand per minute) of pulses from a single photomultiplier, almost all due to dark current and some due to background radioactivity. In order to avoid a large number of accidental associations with the shower trigger on the surface, a two-fold coincidence between the discriminator outputs belonging to the same detector was taken, reducing the detector output rate to 50-150 pulses per minute. Most of these were due to local radioactivity. The chance association rate with EAS triggers was thus reduced to approximately 7.5% of the recorded rate of such associations. The two-fold output from each detector was delayed, using HH-4000 delay cable, by an amount characteristic of of the detector (varying from 2 μs to 10 μs) and mixed with the undelayed pulse. Pairs of pulses from all the four detectors were further mixed and sent to the recording room on the surface by an RG-11/U cable. On the surface the pulse were time sorted and pulses from individual detectors were tagged and stored to record the yes/no information in the event of a trigger.

Two of the scintillators were surrounded by a Neon Flash Tube (NFT) telescope to locate the muon track. Crossed NFT trays were used to get projections of the track in two orthogonal vertical planes. The north-south projection was obtained using two trays of NFT, each of area 2 m^2, separated vertically by 2.25 m with the scintillators between them. Each NFT was 1 m long and 1 cm in diameter. The east-west projection was obtained using three trays of NFT, each of area 2 m^2. Each NFT was 2 m long and 2 cm in diameter. Two trays were placed one below each of the N-S trays and the third between them, just below the scintillators. A schematic diagram of the telescope is shown in figure 3.

Each tray of NFT had four layers of tubes staggered such that a muon passing through the tray would fire at least two tubes, except at the very edge of the tray. The worst case accuracy in the projected angle was $0^{o}.25$. The trays were arranged to be horizontal to better than $0^{o}.1$ and the orthogonality of the N-S and E-W trays was also better than $0^{o}.1$. The

vertical, determined using a plumb line, was also known to the same accuracy.

A coincidence between the pulses from the scintillators surrounded by the telescope and an air shower trigger on the surface generated a pulse which was sent underground through the same cable that was used to bring the underground pulses to the surface. This pulse was used to generate a trigger to apply a high voltage pulse (~13 KV) to the NFT trays and photograph them for later analysis.

A graduated scale, with graduations corresponding to each of the tubes in the lowest layer of each tray, was illuminated and photographed in each event. The scale was placed just below each tray so that for each event the serial number of each tube that has flashed in the lowest layer was known. Knowing the pattern of tubes in each tray, the serial numbers of tubes that flashed in the other layers was also easily obtained. A system of mirrors was used to photograph both the projected tracks on the same frame of the film. The delay between the passage of the muon through the telescope and the application of the high voltage pulse to the flash tubes was ~ 10 μs (which includes the muon travel time from surface to the underground detectors and the cable delay for the pulses from the underground detectors to travel to the surface laboratory and the trigger pulse to travel from the surface to the underground laboratory), sufficiently small to operate the tubes with an efficiency of ~ 85%. With four layers of tubes per tray, the track location efficiency was 96%.

3. Data Recording

In order to collect an adequate number of showers of small size, the triggering system was designed to yield a large area of collection for these showers. This resulted in a high triggering rate and hence a large relative dead time. Thus, it became necessary to operate the array with different triggering systems at different times for showers of different sizes. Moreover, a separate triggering system had to be adopted for collecting showers with a high energy muon in the underground detector because of the small number of these muons per shower. The various triggers employed to record the data are described below.

3.1 Types of Triggers

3.1.1 S (surface) Trigger

Air showers were selected by a three fold coincidence between any set of three adjacent detectors forming an equilateral triangle of side 5 m, among the innermost 37 detectors, with at least three particles in each of them (for part of the runs only the innermost 19 detectors were used for this selection). This trigger selected showers of size 10^4 particles with good efficiency up to 15 m from the center. Though the rate of these triggers was ~ 30 per minute, the actual rate of recording was ~ 5 per minute because of a dead time of 10 s (see section 3.2). In all about 35,000 such triggers were recorded during 120 hours of operation. Most of the showers collected with this trigger were in the size range 5×10^3 to 10^5. No other trigger was on when this trigger was operating.

3.1.2. SD and LS Triggers

The SD and LS (large size) triggers were used to collect showers of

medium and large size respectively. Since the rate of these two triggers was low, dead time effects were minimal. The SD trigger required 10 particles in the central detector and 6 particles in each of three symmetrically placed detectors in the 5 m ring. The size threshold for efficient triggering in this case was 4×10^4 and the trigger rate was 80 per hour. The LS trigger required 15 particles in each of three symmetrically placed detectors in the 20 m ring giving a size threshold of 1.6×10^5 particles and a trigger rate of 10 per hour.

In all about 30,000 SD showers and about 35,000 LS showers were collected during 400 and 3,000 hours respectively.

3.1.3 SU Trigger

Showers associated with high energy muons were selected by a coincidence of the S-trigger pulse and any of the pulses from the underground muon detectors (U pulses). A 6 μs resolving time was used for this coincidence to accommodate the transit time of the muons from the surface to the underground level as well as the pulse transit time through the cable. The rate of U pulses was approximately 600 per minute, which gave rise to SU coincidences purely by chance at the rate of < 0.2 per hour. The observed rate of SU coincidences was ~ 3 per hour. A subset of SU showers, called SUT showers, had at least one muon passing through the telescope. In all about 30,000 SU showers were recorded in 10,000 hours of operation, out of which about 3,000 were SUT showers in which the muon track was unambiguously defined with tracks in all the five NFT trays.

The LS and SU triggers were run concurrently because of their low rates, whereas the S and SD showers were collected in separate runs.

3.2 Recording System and Calibration Procedures

Any of the triggers outlined above initiated the recording of the shower information. The density information from all the detectors, the fast timing information, the yes/no information from the underground detectors, the date and time of arrival of the shower, information regarding non-working detectors and some house keeping information were all recorded on magnetic tape using a TDC-12 on-line computer [9]. The logarithmic output from each detector, available as analog DC level on memory capacitors, was sequentially fed to a 12-bit analog to digital converter (ADC) through a 90 channel analog multiplexer and the digitised output was read into the memory of the TDC-12 computer under program control. Once the recording of the shower data was over, the computer reverted to routine monitoring of the surface detectors (see later). The system dead time was 10 seconds. A block diagram of the recording system is shown in figure 4.

The TDC-12 computer is a second generation, general purpose digital computer with a 12-bit word length, 2 μs cycle time, 500 ns access time and a 12 level priority interrupt, suitable for real time applications. The processor, an 8 K word memory, two magnetic tape units and an ASR-35 teletype formed the complete system.

During on-line operation the computer was used in two modes, the EVENT mode (EM) and the CALIBRATION mode (CM). In the CM, linear outputs from the 76 surface scintillators (70 density detectors, 4 low energy muon detectors and 2 energy flow detectors) were selected sequentially, one at a time, through an analog multiplexer and fed to a pulse stretching circuit which sampled and held the pulse height for digitisation by the ADC under program

control. On 'end of conversion' signal from the ADC, the digital information was read into the accumulator and a pulse height histogram was formed and stored in the memory. The histogram was formed during a one minute live time for each detector sequentially. At the end of the one minute period, the pulse height corresponding to the passage of two particles through the detector, which corresponds to an integral counting rate of 3100 pulses per minute (1330 per minute for the 1 m^2 area density detectors and 2700 per minute for the low energy muon detectors) was estimated by interpolation. The interpolation accuracy was 20 mV, the ADC accuracy. The interpolated pulse height for the current period along with that of the previous sampling and a message, if these two differed by more than 20%, were all printed out and the computer switched to monitoring the next detector. The current values of the interpolated pulse height for all the detectors was always resident in the memory. These were fed into the memory before the start of the run and were continuously updated in the CM. The monitoring of each detector was, thus, carried out every 1.5 hours assessing its performance. This monitoring routine formed the background program for on-line operation, with the EVENT interrupt given top priority. The occurrence of any trigger mentioned earlier was termed an EVENT. When an EVENT occurred the monitoring was suspended, the data pertaining to the EVENT recorded and the program reverted back to resume monitoring from where it was suspended due to the EVENT interrupt. A crystal clock oscillator provided clock signals every 100 ms to the computer for time keeping.

The relation between the logarithmic and linear outputs of each of the amplifiers was determined using LL (log-linear) calibration, which was normally done off-line, but could be done on-line also. This mode was selected by a manual switch on the console. An additional amplifier, linear over four decades in four stages, was used to measure the pulse input to the logarithmic amplifier. The same input was given to the amplifier under check and the additional amplifier. On command, the logarithmic output and the four linear outputs from the additional amplifier were printed out by the computer. The relative gains of the four stages of the additional amplifier with respect to the linear output of the amplifier under check were measured and fed to the computer before each calibration. All linear outputs were converted to this scale and printed out. The integral pulse height spectrum measured during routine monitoring in the CM was also obtained using the same linear scale.

3.3 Calibration of Detectors

The average pulse height due to the passage of vertical single minimum ionising muons, selected using a narrow angle ($< 12^\circ$) GM counter telescope, was determined for each type (2.25 m^2 and 1 m^2) of detector separately. As the average pulse height could depend on the position at which the muon has traversed the detector, this average was determined at various distances from the center of the detector. It was found that the average pulse height varied from the center to the edge only by 15%. From these measurements, the average for the entire detector was estimated and the position in the detector where the average pulse height would be equal to the detector average, was determined. The mean of the pulse height distribution, obtained with the narrow angle telescope, at this average position was then determined with good accuracy (<1%) and was thereafter used as the response of the detector for vertical single particles. All distributions were truncated at twice the peak value for determining the averages.

The density spectrum, ie. the integral pulse height distribution, for the omni-directional cosmic rays passing through the detector, was then determined up to 100 particles. This spectrum could be well approximated by

a power law of slope -3.0. The rate of pulses above the two particle pulse height, H_2 (equal to twice the average single muon pulse height), was obtained from this spectrum and was thereafter used for monitoring the detector. The level of two particles was chosen as the optimum to keep the noise contribution to a minimum and to obtain a reasonably accurate density spectrum in that region during one minute of monitoring time.

The LL calibration was done, for all detectors, at the beginning of the experiment using a light emitting diode to cover a dynamic range of four decades. The constancy of the log-linear relation was checked by repeating the LL calibration every three months, using cosmic rays.

From the LL calibration and the monitoring data (H_2 values), the logarithmic output, recorded in the events, was converted into number of particles in the detector. The LL relationship was parameterised as

$$P = A \log (L) + B \qquad \ldots\ldots 1$$

where L is the linear pulse height corresponding to a logarithmic output P. A and B were constants determined for each detector separately. The density, Δ (particles m^{-2}), was then given by

$$\Delta = (2/H_2 a)\ 10^{(P-B)/A} \quad (m^{-2}) \qquad \ldots\ldots 2$$

where a is the area of the detector. Figures 5(a) and 5(b) respectively show a typical distribution for single particles and LL calibration for a 2.25 m^2 detector using cosmic rays.

For the high energy muon detectors, 'in situ' calibration of the response of the detector using single muons was not practicable due to the low flux of muons. A standard detector identical to the ones used underground was set up on the surface. The photomultiplier amplifier system to be used underground was used with this detector and the high voltage for the photomultipliers and the amplifier gains were adjusted to yield an efficiency of > 90% for detecting single muons, selected by the narrow angle GM counter telescope at the average position in the detector. The high voltage and the two fold counting rates were monitored underground for constancy. If any detector showed deviations from constancy, its photomultiplier amplifier system was brought up for recalibration. The overall efficiency of the underground detectors for detecting single particles was ~ 85%.

In the case of the fast timing detectors, the linear relationship between the delay to be measured and the digital output as well as the output corresponding to zero delay were determined by operating all the five photomultipliers viewing the same scintillator (mounting them on the same scintillator tank) and using the same set of cables and electronics. Triggering on cosmic rays through the tank, the output for zero delay was determined in a straightforward way. The delay-output relation was obtained by introducing known delays in the form of known lengths of RG-11/U cable. A delay range of 100 ns was covered. The photomultiplier high voltages were set for 95% efficiency for detecting single muons, using the narrow angle Geiger telescope.

4. Data Analysis

4.1 Estimation of Shower Parameters

The zenith and azimuthal angles of the shower arrival direction were obtained by fitting the arrival time differences to a plane shower front moving along the shower axis with the velocity of light, using a straight forward least square procedure.

For each shower, the density information available in the distance range 2 m to 60 m was fitted to the Nishimura-Kamata-Greisen (NKG) function [10], given by

$$\Delta(r) = \frac{N}{2\pi r_o^2} \frac{\Gamma(s-2)}{\Gamma(s)\,\Gamma(4.5-2s)} \left(\frac{r}{r_o}\right)^{(s-2)} \left(1+\frac{r}{r_o}\right)^{(s-4.5)} \quad \ldots\ldots 3$$

where $\Delta(r)$ is the density of particles at a distance r meters from the core, s the age parameter, N the shower size and r_o the Moliere unit taken to be 96 m corresponding to the atmospheric depth of KGF. N, s and the coordinates x_o, y_o of the shower core in the array plane were determined for each shower by minimising the function

$$\chi^2(N,s,x_o,y_o) = \sum_{i=1}^{n} \omega_i \, (\Delta_{oi} - \Delta_{ei})^2 \quad \ldots\ldots 4$$

where $$\omega_i = \sigma_i^{-2} = [\, a_i \Delta_{ei} + (0.2 a_i \Delta_{ei})^2 \,]^{-1} \quad \ldots\ldots 5$$

using the method of steepest descent, similar to the one used by the MIT group [11]. Here Δ_{oi} and Δ_{ei} are the observed and expected (according to the NKG function) densities and a_i and ω_i are the area and the weight factor for the i th detector respectively. The first term in equation 5 corresponds to the statistical error and the second one to the systematic error, which is estimated to be 20%. For computational convenience, only the first term was included for densities less than $25/a_i$ and only the second one beyond, as these terms dominate in the corresponding regions. The minimisation was carried out on the CDC 3600 computer system at the Tata Institute of Fundamental Research, using a FORTRAN program developed for the purpose.

An important feature of the present experiment is the accuracy with which parameters of showers with size as low as 10^4 particles have been obtained. At these sizes the density of particles expected beyond a few meters from the core, where bulk of the data was available, was only a few particles per m^2. So a large number of detectors record no particles due to fluctuations that carry the observed density below threshold. If these 'zero density' detectors are ignored during analysis, an unduly flat lateral distribution would be obtained for the shower as only those detectors which showed an upward fluctuation would be used. However if the number of detectors with near threshold densities was small, using them in

the analysis would have steepened the distribution in a large fraction of the showers, the fraction depending on the smallest expected density. In the present experiment a fairly large number (~ 25) of detectors with near threshold densities were available for showers of size about 10^4 particles and therefore we could use the 'zero density' detectors for analysis and estimate the parameters accurately even for very low sizes. The accuracy of the estimated parameters at these low sizes has been determined using artificial showers, analysed using the same procedure as for the real showers, to be described in section 4.3.

4.2 Classification of Showers

All the data have been primarily classified according to the estimated size. Table 1 summarises the several aspects on which information has been obtained from the present experiment. Since showers are classified according to size, the migration of showers from one size group to the other, due to errors in the analysis, has to be carefully taken into account. This has been done using the analysis of artificial showers.

4.3 Estimation of errors

The iterative minimisation procedure described earlier, does not lend itself easily to a determination of the errors in the estimated parameters. An easier and more straightforward way, for this purpose, is the use of 'artificial showers'. An 'artificial shower' is a set of 'observed' densities in the detectors of the EAS array, constructed from the NKG distribution and the estimated fluctuations, with the shower parameters (size N_t, age s_t and coordinates of the core x_t, y_t) assumed 'apriori'. Estimating the shower parameters using this set of densities by the iterative procedure gave an estimate of the deviations of the estimated parameters from the true ones.

The artificial showers were generated using Monte Carlo method. Because of the circular symmetry of the array, the errors on the estimated parameters are expected to be dependent only on the distance of the shower core from the center of the array and not on the actual core location. The array was, therefore, divided into a number of annular rings around the array center, each of width 5 m, up to a distance of 20 m - the distance up to which most of the real showers were accepted for final analysis. Showers were allowed to fall uniformly in each ring. For each set of values of N_t and s_t, 400 showers were generated in each annular ring. For each shower, a set of 'observed' densities in all the detectors were generated by imposing fluctuations, using Monte Carlo technique, on the average densities calculated from the NKG function. The fluctuations were sampled from a Gaussian distribution of width given by equation 5. These densities were fed to the shower minimisation program as if they were from a real shower and the shower parameters N, s, x_o and y_o were estimated. The deviation histograms on $\delta x = (x_o - x_t)$, $\delta y = (y_o - y_t)$, $\delta s = (s - s_t)$ and $\delta(\log N) = (\log N - \log N_t)$, then, gave the standard errors on the estimated parameters.

Tables 2a and 2b show the cross correlation of the estimated parameters N and s for some selected values of N_t and s_t. The N_t, s_t values and the inner and outer radii (r_1 and r_2 respectively) of the annular ring within which the cores are selected are also shown in the table. The numbers given in the main body of the table are the fraction of showers in each bin of N and s. It can be seen that there is a general trend of N being overestimated when s is overestimated and vice versa, particularly for the smallest and the flattest showers, as expected. However, the

fraction of such showers is not very large, and for larger and steeper showers this effect is quite small. Figures 6,7 and 8 respectively show the δx, δs and $\delta(\log N)$ distributions for the same group of showers as in Table 2. The sample standard deviations σ_x, σ_y, σ_s and $\sigma_{\log N}$ for these showers are shown in Table 3. It can be seen that σ_x and σ_y are less than a meter and $\sigma_s < 0.15$ in most of the cases.

4.4 Triggering Efficiency of the Array

The triggering criteria discussed in section 3.1 set the threshold for showers to be recorded by the recording system. For further analysis, additional software selection criteria were imposed at the time of analysis. The criterion was size dependent and required a sevenfold (four fold for showers in the estimated size between 2×10^4 and 4×10^4) coincidence of detectors forming the center and six vertices of a regular hexagon of side 5 m. The minimum numbers of particles required in each detector for different size groups are given in Table 4. It may be noted that the software selection criterion selects only a subset of the showers selected by the hardware selection criterion. For each of these selection criteria, the efficiency for detecting showers of size N_t and age s_t was estimated as a function of the distance of the shower core from the center of the array. As before, showers with fixed N_t and s_t were selected uniformly in an annular ring (inner radius r_1 and outer radius r_2). For each shower the 'observed density' was calculated for each of the detectors in the selection system by imposing fluctuations on the densities expected from the NKG function and the selection criterion was applied. The shower was 'detected' if the criterion was satisfied. The efficiency estimates were based on 1000 showers generated in each annular ring, whose width varied from 0.5 m for the lowest sizes to 4 m for the highest, and for each set of values of N_t and s_t which were respectively varied from 2.5×10^3 to 1.28×10^6 in steps of a factor of 2 and from 0.1 to 1.9 in steps of 0.1. This efficiency map was obtained up to a distance from the center of the array where the efficiency fell to ~ 1%. The maps clearly showed that showers less than 10^4 could not be detected with 100% efficiency at any point in the array, setting the size threshold. For all sizes and ages we have calculated the value of r_{90}, the distance up to which showers were detected with an efficiency exceeding 90% and accepted all showers within r_{90} for further analysis. The overall efficiency within this distance, however, is 99%. Table 5 gives the r_{90} values for various size and age groups obtained taking into account the relevant triggering (S, SD or LS) criterion for the different size groups. The maximum value of r_{90} actually used was 40 m even though the calculated r_{90} value exceeds this as the detector spacing becomes larger beyond this distance.

4.5 Effect of errors on features of air showers

As is the case in any air shower experiment, the features of air showers obtained using the size and age as the primary classifiers, would be affected to a certain extent by the errors in the estimation of the shower parameters, which should be taken into account in the interpretation of the results. The extent to which they will be affected can be described by a transfer function, which is dependent on the geometry of the array and the procedure for estimating the shower parameters. This function, $G(N_t, s_t, x_t, y_t, N, s, x_o, y_o)$, relates the true parameters of the shower (N_t, s_t, x_t, y_t) to the estimated ones (N, s, x_o, y_o) and is defined as the probability that a shower with true parameters N_t, s_t, x_t, y_t will be estimated to have parameters N, s, x_o, y_o. Note that the function G depends on the core location also as seen from table 3 and figures 6, 7 and 8, which is characteristic of any air shower array - particularly if the

detector separation increases with distance from the center of the array.

Consider, for example, the size spectrum of EAS, f(N,s) dN ds, which is the flux of showers (m^{-2} s^{-1} sr^{-1}) of size between N and N+dN and age between s and s+ds. This quantity is experimentally obtained by classifying the showers by the estimated size and age, N and s, and collecting all showers that fell within a certain area A(N,s) (m^2), (usually the area over which showers of this size and age are detected with 100% efficiency - see section 4.4) during a time T (sec). If n(N,s) were the number of showers so collected over a solid angle Ω steradians, then the size spectrum is given by

$$f_{obs}(N)\, dN = dN \int n(N,s)/(\, A(N,s)T\Omega\,)\, ds \qquad \ldots\ldots\ 6$$

However, this is not the true spectrum as it is influenced by the errors in the estimation of N and s as well as by the migration of showers into and out of the area A(N,s) because of core location errors. It is related to the true spectrum $f_t(N_t,s_t)$ by

$$f_{obs}(N)\, dN = \int_{x_o}\int_{y_o}\int_{x_t}\int_{y_t}\int_{N_t}\int_{s_t}\int_{s} (1/A(N,s))\, f_t(N_t,s_t)\, \varepsilon(N_t,s_t,x_t,y_t)$$

$$G(N_t,s_t,x_t,y_t,N,s,x_o,y_o)\ dN_t\, ds_t\, dx_t\, dy_t\, dx_o\, dy_o\, ds \qquad \ldots\ldots\ 7$$

where $\varepsilon(N_t,s_t,x_t,y_t)$ is the efficiency of detecting a shower with parameters (N_t, s_t, x_t, y_t) and A(N,s) is the area over which the showers are collected. This equation forms the basis for calculating any of the expected EAS properties, e.g. the size spectrum, the relationship between the muon and electron sizes (N_μ - N_e) etc. Equation 7 can be rewritten as

$$f_{obs}(N)\, dN = \int_{s} \frac{ds}{A(N,s)} \int_{N_t}\int_{s_t} f_t(N_t,s_t)\, p(N_t,s_t,N,S)\, dN_t\, ds_t \qquad \ldots\ldots\ 8$$

where

$$p(N_t,s_t,N,s) = \int_{x_o}\int_{y_o}\int_{x_t}\int_{y_t} \varepsilon(N_t,s_t,x_t,y_t)\, G(N_t,s_t,x_t,y_t,N,s,x_o,y_o)$$

$$dx_o\, dy_o\, dx_t\, dy_t \qquad \ldots\ldots\ 9$$

The integrals in equation 9 are dependent on the geometry of the array, the selection criteria (through ε) and the errors in the estimation of shower parameters (through G). As the evaluation of the function G over the entire parameter space and subsequent integration takes a lot of computer time the integrals are replaced by summations and evaluated using the Monte Carlo method. As before, showers were allowed to be incident

uniformly over an area, A_t, covering the range of x_t and y_t and extending up to a distance, r_m, from the center of the array where $\varepsilon \leq 1\%$, densities in the triggering detectors calculated, fluctuations imposed. Showers satisfying the selection criteria were analysed as if they were real showers and the parameters N, s, x_o, y_o were estimated. The range of N_t covered, from 2.5×10^3 to 6.4×10^5, was divided into 48 equal logarithmic intervals and the range of 0.4 to 1.8 in s was covered in 28 bins of width 0.05 each. For computational convenience, only four values of r_m - 20m, 50m, 100m and 150m - corresponding to the size intervals $(0.25\text{-}1)10^4$, $(1\text{-}4)10^4$, $(0.4\text{-}1.6)10^5$ and $(1.6\text{-}6.4)10^5$ respectively - were used. Showers whose estimated cores were within the area, A(N,s) (see table 5), were then used for calculating $p(N_t,s_t,N,s)$. If $n(N_t,s_t,N,s)$ were the number of showers so picked (usually 20) with size N and age s out of $n_g(N_t,s_t,N,s)$ showers generated over an area A_t ($= \pi r_m^2$) with size N_t and age s_t, then

$$p(N_t,s_t,N,s) = n(N_t,s_t,N,s)\ A_t\ /\ n_g(N_t,s_t) \qquad \ldots\ldots\ 10$$

Substituting this in equation 8, $f_{obs}(N)$ can be estimated from a given $f_t(N_t,s_t)$. Figure 9 shows the input and output size spectra for an input spectrum, $f_t(N_t,s_t) \propto N_t^{-2.4}$. It is seen that the estimated fluxes are somewhat overestimated while the exponent remains the same. This has to be taken into account when the spectrum predicted by theory is compared with the experimental data.

For any other parameter, g(N,s), of the showers we can generalise equation 8 and estimate the expected average value of the parameter as

$$g_{exp}(N,s) = \frac{\int_{N_t}\int_{s_t} g(N_t,s_t)\ f_t(N_t,s_t)\ p(N_t,s_t,N,s)\ dN_t\ ds_t}{\int_{N_t}\int_{s_t} f_t(N_t,s_t)\ p(N_t,s_t,N,s)\ dN_t\ ds_t} \qquad \ldots\ldots\ 11$$

An example of such a parameter studied in this experiment is the number of muons of energy > 220 GeV [12,13].

4.6 Analysis of the High Energy Muon Data

Data on high energy muons were provided by the four scintillators and the Neon Flash Tube telescope located 270 m underground. The overburden of rock above these detectors corresponds to 815 hg cm^{-2} of Kolar rock, which is essentially made of Hornblende schist and has a mean density of 3.02 g cm^{-3}, $\langle Z/A \rangle = 0.495$ and $\langle Z^2/A \rangle = 6.31$ [14]. The minimum energy required for a muon to reach this depth depends upon the energy loss. Though fluctuations in the energy loss are not very important at this depth, Krishnaswamy [15] calculated the survival probability of muons as a function of energy taking them into account. Figure 10 shows this plot. Integrating the product of the survival probability and the differential energy spectrum of muons in air showers, taken to be $\propto E^{-2.5}$, gave the number of muons arriving at that depth. The energy at which the integral number of muons is equal to this number is the effective threshold energy and is estimated to be 220 GeV.

The determination of the lateral distribution of muons requires the measurement of the distance of the muon from the core. The core location is determined from the shower parameter analysis to an accuracy of 1 m in the

region of the array where the shower detection efficiency is > 90% (see table 3). The location of the muon in the array coordinate system is given by the NFT data. From the known positions of the flashed tubes in the various layers in the NFT telescope, the projected trajectories of the muon in the two orthogonal planes were obtained. The muon trajectory in space, its point of intersection with the array plane and the distance of the muon from the core in the shower plane, assuming the muon arrival direction and the shower arrival direction are same (since the energy of the muon is large the two directions are same within a fraction of a degree - the angle between the two is $\sim p_t/E$, where p_t is ~ 0.3 GeV/c).

The various sources of error in the determination of the distance of the muon from the shower core are the error due to the finite size of the NFTs and the geometry of the telescope, multiple coulomb scattering of the muon in the rock above the underground telescope, the core location errors and finally the deflection of the muons in the geomagnetic field. The last source has to be taken into account, if it is large, when one compares the experimental lateral distribution with theoretical predictions which do not take this deflection into account. These errors have been estimated by Srikantha Rao [16] and are briefly discussed here.

Because of the finite diameter of the NFTs, several trajectories are possible for a given configuration of the tubes in the various trays. However, the error in the projected angles is small since the diameter of the tubes is small (1 cm and 2 cm), the tubes in each tray are staggered and the top and bottom trays in each view are separated by 2.25 m and it is estimated to be $0^o.1$. The error in the projected angles due to multiple Coulomb scattering is estimated to be $0^o.17$ taking into account the energy loss of the muons in the rock and the energy spectrum of muons in air showers. The corresponding error in the location of the muon in surface array plane due to the combined error in the projected angles, is o.9 m. This combined with an error of 1 m in the core location (see table 3) results in an error of 1.9 m in the core distance of the muon in the shower plane. The deflection of the muons in the geomagnetic field is estimated to be 1.2 m taking into account their energy spectrum. The effective error for purposes of comparing the experimental data on the lateral distribution of muons with theoretical predictions which do not take the magnetic deflection into account is, therefore, 2.2 m. It should be noted that this error is independent of the core muon distance since the error in core location is nearly constant over the area where showers are accepted for final analysis (efficiency > 90%) and the error in the muon location is also nearly independent of the zenith angle at least up to 20^o (corresponding to a core muon distance of ~ 100 m), the maximum recorded angle in the data.

5. Conclusions

The extensive air shower array along with an underground neon flash tube telescope to detect muons of energy > 220 GeV, operated at Kolar Gold Fields, India, is described. The computerised recording system and the detector monitoring and calibration procedures are discussed in detail. The procedure of analysis for obtaining the shower parameters and the distance of the high energy muon from the shower core is described. An important feature of the experiment is the closely packed central region of the array, where large area detectors were deployed at a mutual separation of 5 m and within which small showers were accepted for final analysis, and the availability of a large number of density measurements near the threshold density. This feature enabled the parameters to be estimated accurately for sizes as small as 10^4 particles. The typical errors for the finally accepted showers are 1 m in the core location, 30% in shower size, 0.1 in

the age parameter and 2.2 m in the core-muon distance.

Acknowledgements

We thank the management and staff of the Bharat Gold Mines Limited for the excellent facilities and cooperation extended by them, without which the experiment could not have been carried out. Messrs. P.B.Subramaniam and A.M.Gurumurthy installed and maintained the computer system and the interface electronics. Mr. A.V.John developed the complete software for the on-line recording and monitoring system and several utility programs. Messrs. M.A.Patil, S.G.Khairatkar, A.D.Ranpura, S.D.Samuel and other staff members contributed extensively in the design and maintenance of all the detectors and the associated electronics. Dr.V.S.Narasimham and Messrs. H.D.Salvekar and R.M.Wankar helped in the construction of the NFT telescope. We thank all of them for their contributions.

References

1. B.V.Sreekantan, Proceedings of the International Cosmic Ray Conference, Jaipur, 4 (1963) 143.

2. B.K.Chatterjee, S.Lal, T.Matano, G.T.Murthy, S.Naranan, K.Sivaprasad, B.V.Sreekantan, M.V.S.Rao and P.R.Vishwanath, Proceedings of the International Cosmic Ray Conference, London, 2 (1965) 627.

3. B.V.Sreekantan, Proceedings of the 12th International Cosmic Ray Conference, Hobart, 7 (1971) 2706.

4. S.Naranan, K.Sivaprasad, B.V.Sreekantan and M.V.S.Rao, Proceedings of the 13th International Cosmic Ray Conference, Denver, 3 (1973) 1872.

5. B.S.Acharya, M.V.S.Rao, K.Sivaprasad and Srikantha Rao, Conference Papers, Kyoto, 16th International Cosmic Ray Conference, 8 (1979) 312.

6. B.S.Acharya, S.Naranan, M.V.S.Rao, K.Sivaprasad, B.V.Sreekantan and Srikantha Rao, Conference Papers, 16th International Cosmic Ray Conference, Kyoto, 13 (1979) 272.

7. N.L.Grigorov, Yu.V.Gubin, I.D,Rapoport, I.A.Savenko, B.M.Yakovlev, V.V.Akimov and V.E.Nesterov, Proceedings of the 12th International Cosmic Ray Conference, Hobart, 5 (1971) 1746.

8. K.Suga, G.Clark and I.Escobar, Rev. Sci. Inst., 32 (1961) 1187.

9. S.Naranan, M.V.S.Rao, K.Sivaprasad and P.B.Subramaniam, Conference Papers, 14th International Cosmic Ray Conference, Munich, 9 (1975) 3343.

10. K.Greisen, Ann. Rev. Nucl. Sci., 10 (1960) 63.

11. F.Scherb, MIT Tech. Rep. No. 71 (1959).

12. B.S.Acharya, S.Naranan, M.V.S.Rao, K.Sivaprasad, B.V.Sreekantan and Srikantha Rao, Conference Papers, 16th International Cosmic Ray Conference, Kyoto, 8 (1979) 304.

13. B.S.Acharya, S.Naranan, M.V.S.Rao, K.Sivaprasad, B.V.Sreekantan and Srikantha Rao, Conference Papers, 17th International Cosmic Ray Conference, Paris, 9 (1981) 162.

14. P V.Ramana Murthy, Ph.D. Thesis (unpublished), University of Bombay, 1962.

15. M.R.Krishnaswamy, Ph.D. Thesis (unpublished), University of Bombay, 1981.

16. Srikantha Rao, Ph.D. Thesis (unpublished), University of Bombay, 1981.

Table Headings

1. The different types of triggers and information obtained from them.

2. Fraction of showers with different estimated values of N and s for some representative values of N_t and s_t in various annular rings of radii r_1 and r_2.

3. RMS deviations of the estimated parameters from the true ones.

4. Software selection criteria imposed at the time of analysis.

5. Radii, r_{90}, of circular areas with efficiency > 90%, over which showers of different size and age parameters are accepted for final analysis.

Figure Captions

1. The Extensive Air Shower array at Kolar Gold Fields. The inset shows the location of the underground NFT telescope with respect to the surface array.

2. Expanded view of the central region of the EAS array showing the positions of the underground detectors projected on to the plane of the surface array. Underground detectors 1 and 2 are located inside the NFT telescope.

3. Schematic view of the underground neon flash tube telescope. The staggering of the NFT tubes is also shown in the expanded view.

4. Block diagram of the computerised recording and monitoring system.

5. (a) Single particle response of a 2.25 m^2 density detector obtained with minimum ionising cosmic ray muons selected by a narrow angle GM counter telescope.

   (b) A typical log-linear (LL) calibration for one of the 2.25 m^2 density detectors.

6. Distribution of deviations in core location ($x_o - x_t$), due to the fitting procedure, for some typical values of the true parameters.

   (a) to (f) : $N_t = 10^4$ and (g) to (l) : $N_t = 8 \times 10^4$
   (a), (b) and (c) : $r_1 = 0$ m and $r_2 = 5$ m.
   (d), (e) and (f) : $r_1 = 10$ m and $r_2 = 15$ m.
   (g), (h) and (i) : $r_1 = 5$ m and $r_2 = 10$ m.
   (j), (k) and (l) : $r_1 = 15$ m and $r_2 = 20$ m.
   (a), (d), (g) and (j) : $s_t = 0.6$
   (b), (e), (h) and (k) : $s_t = 1.0$
   (c), (f), (i) and (l) : $s_t = 1.4$

7. Distribution of deviations in the age parameter ($s_o - s_t$), due to the fitting procedure, for some typical values of the true parameters. Explanations for the symbols are the same as in figure 6.

8. Distribution of deviations in shower size ($\log(N/N_t)$), due to the fitting procedure, for some typical values of the true parameters. Explanations for the symbols are the same as in figure 6.

9. The assumed (continuous line) and the estimated (dashed line) size spectra from the shower analysis procedure.

10. The survival probability at a depth of 815 hg cm^{-2} of Kolar rock as a function of the energy of the muon on the surface.

Table 1. The different types of triggers and information obtained from them.

Trigger	Information obtained	Size range
S, SD & LS	1. Size spectrum	10^4-10^7
	2. Age distribution	10^4-10^7
	3. Low energy muon density	10^4-10^7
S & SUT	1. Lateral distribution and total number of muons of energy > 220 GeV	10^4-3.2×10^5
SUT	1. Low energy muon density	10^4-3.2×10^5
	2. Correlation between low energy muon density and the distance of the high energy muon	
S, SD, LS & SU	1. Total number of high energy muons	10^4-10^7

Table 2. Fraction of showers with different estimated values of N and s for some representative values of N_t and s_t in various annular rings of radii r_1 and r_2.

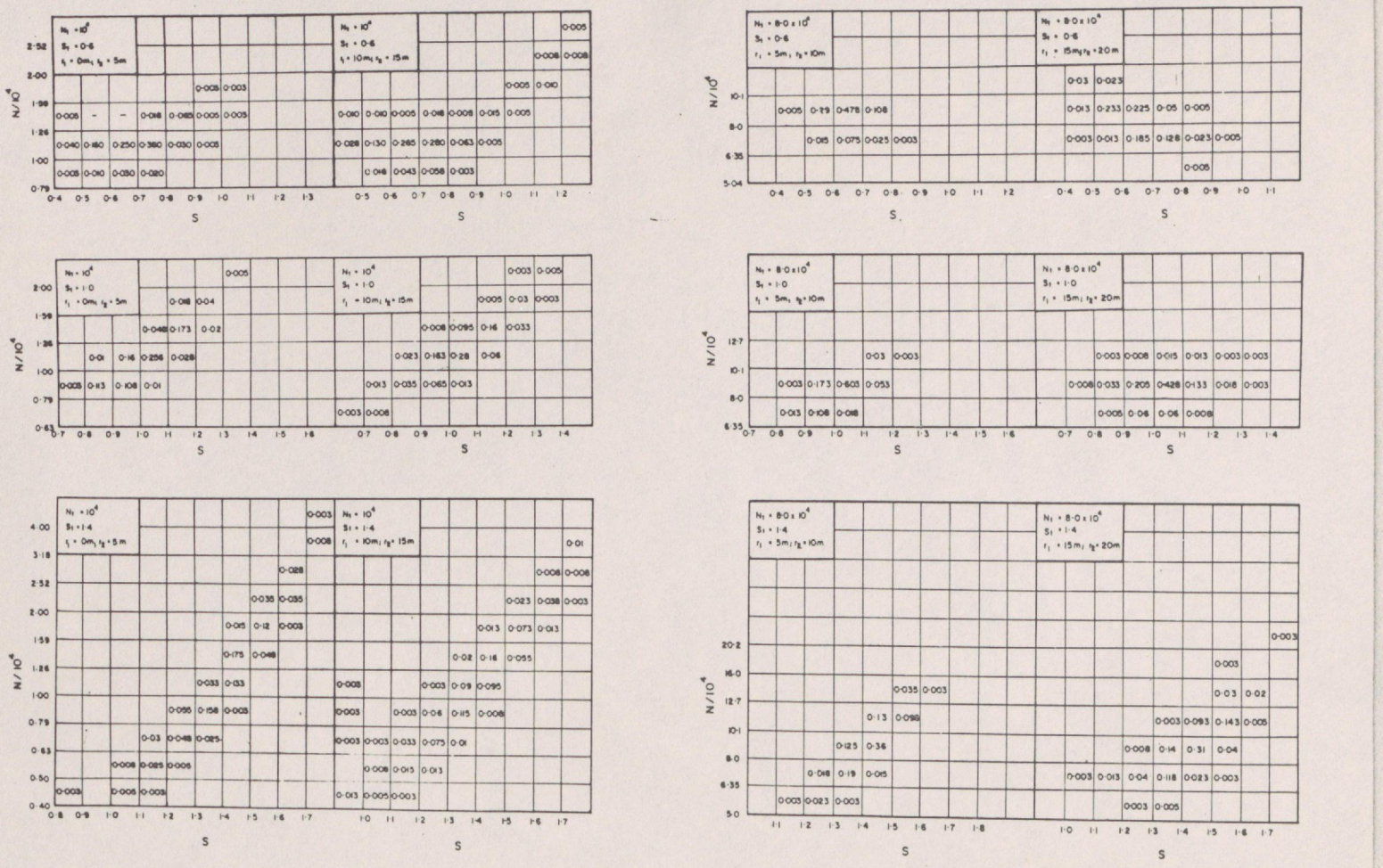

Table 3. RMS deviations of the estimated parameters from the true ones.

N_t	s_t	r_1 (m)	r_2 (m)	σ_x (m)	σ_y (m)	$\sigma_{\log N}$	σ_s
10^4	0.6	0	5	0.38	0.38	0.028	0.11
10^4	1.0	0	5	0.51	0.45	0.081	0.11
10^4	1.4	0	5	1.05	1.07	0.170	0.14
10^4	0.6	10	15	0.47	0.55	0.066	0.14
10^4	1.0	10	15	0.74	0.71	0.075	0.12
10^4	1.4	10	15	1.50	1.50	0.170	0.17
8×10^4	0.6	5	10	0.26	0.26	0.018	0.06
8×10^4	1.0	5	10	0.36	0.37	0.035	0.06
8×10^4	1.4	5	10	0.75	0.65	0.078	0.07
8×10^4	0.6	15	20	0.66	0.66	0.060	0.09
8×10^4	1.0	15	20	0.87	0.86	0.030	0.08
8×10^4	1.4	15	20	1.60	1.50	0.080	0.09

Table 4. Software selection criteria imposed at the time of analysis

Size range	Coincidence Level	Threshold (particles/detector)	
		Center	Corner
$(2-4)10^4$	4-fold	6	3
$(4-8)10^4$	7-fold	6	6
$> 8\times10^4$	7-fold	12	6

Table 5. Radii, r_{90} (m), of circular areas with efficiency > 90%, over which showers of different size and age parameters are accepted for final analysis

Size \ s	0.6-0.8	0.8-1.2	1.2-1.4	1.4-1.6
$(1-2)10^4$	12.0	15.0	10.0	8.0
$(2-4)10^4$	12.0	15.0	10.6	10.0
$(4-8)10^4$	12.0	20.0	14.1	10.6
$(8-16)10^4$	12.0	20.0	14.1	12.0
$> 1.6\times10^5$	12.0	40.0	22.4	20.0

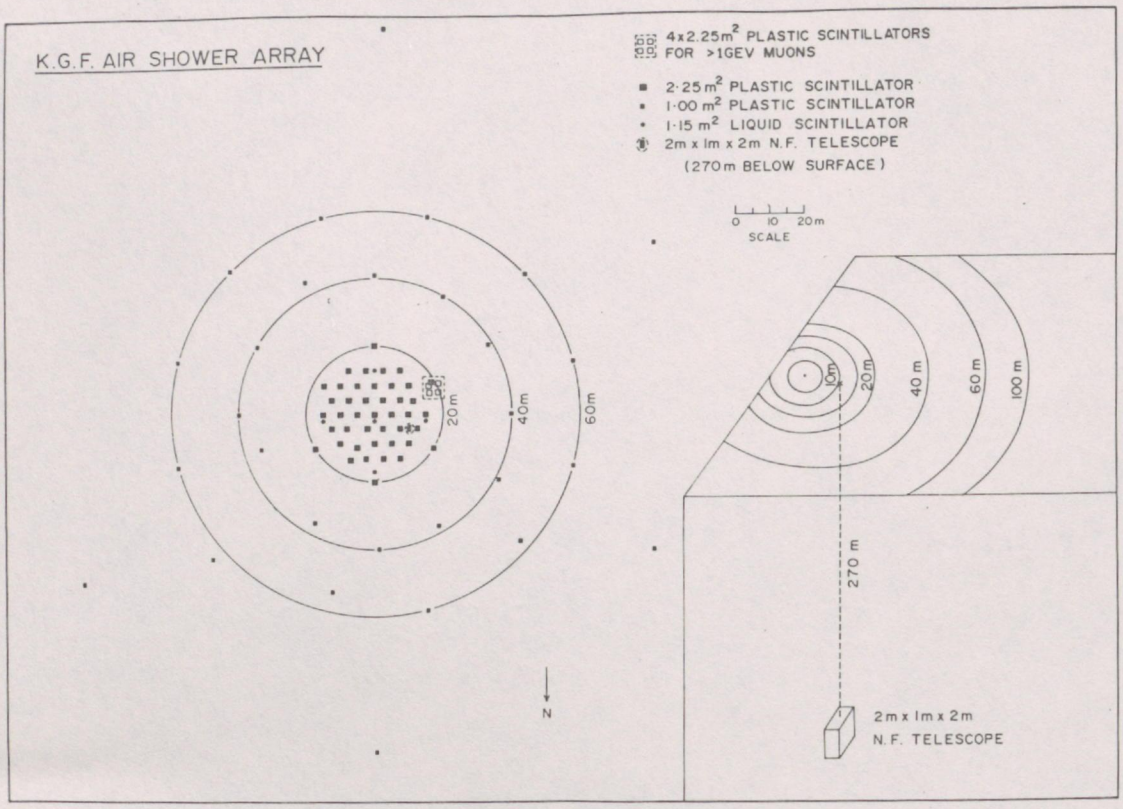

Figure 1. The Extensive Air Shower array at Kolar Gold Fields. The inset shows the location of the underground NFT telescope with respect to the surface array.

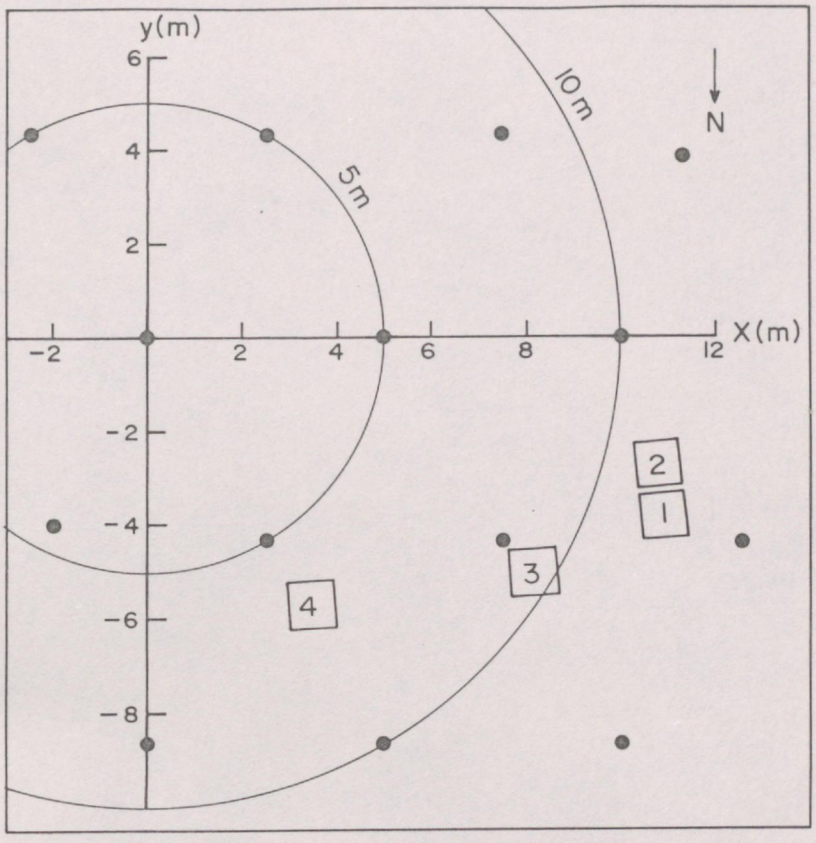

Figure 2. Expanded view of the central region of the EAS array showing the positions of the underground detectors projected on to the plane of the surface array. Underground detectors 1 and 2 are located inside the NFT telescope.

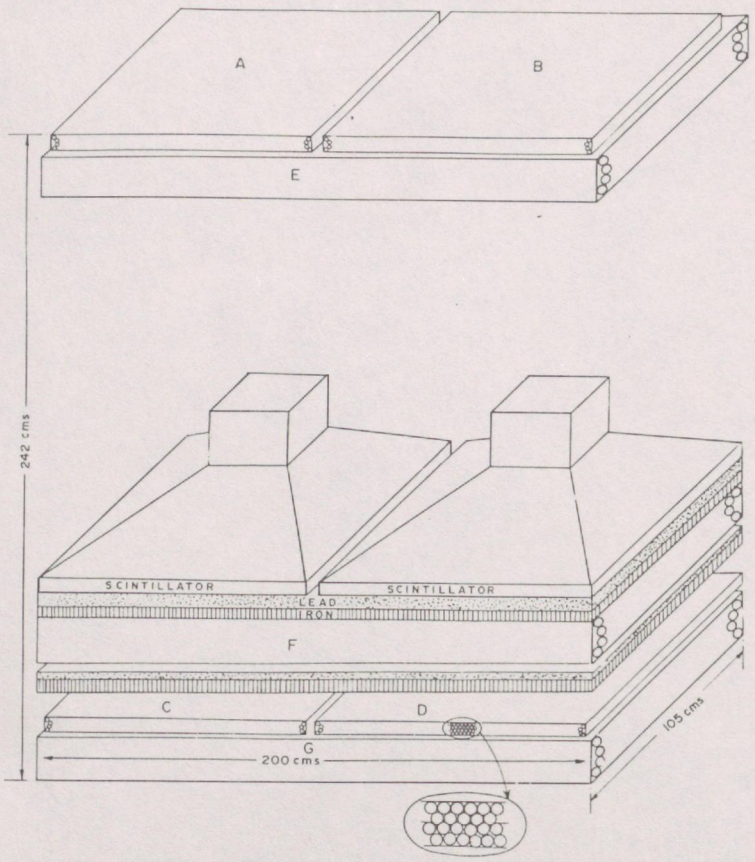

Figure 3.Schematic view of the underground neon flash tube telescope. The staggering of the NFT tubes is also shown in the expanded view.

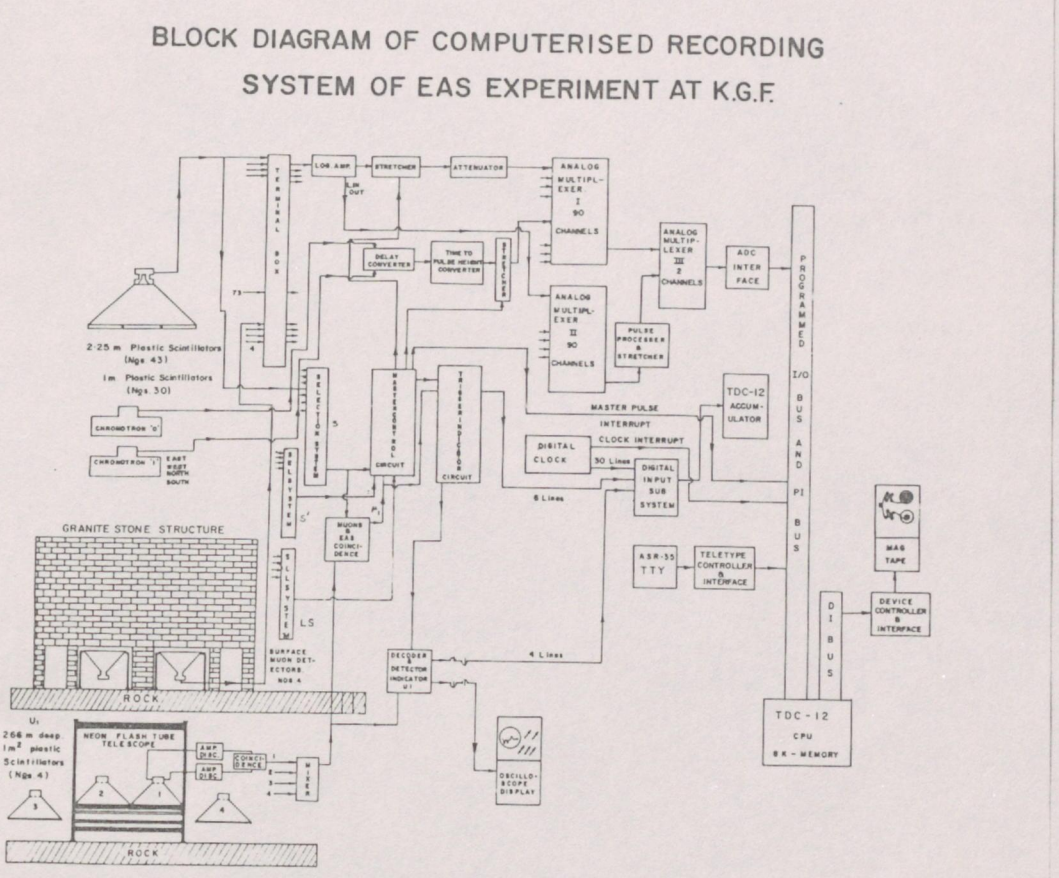

Figure 4.Block diagram of the computerised recording and monitoring system.

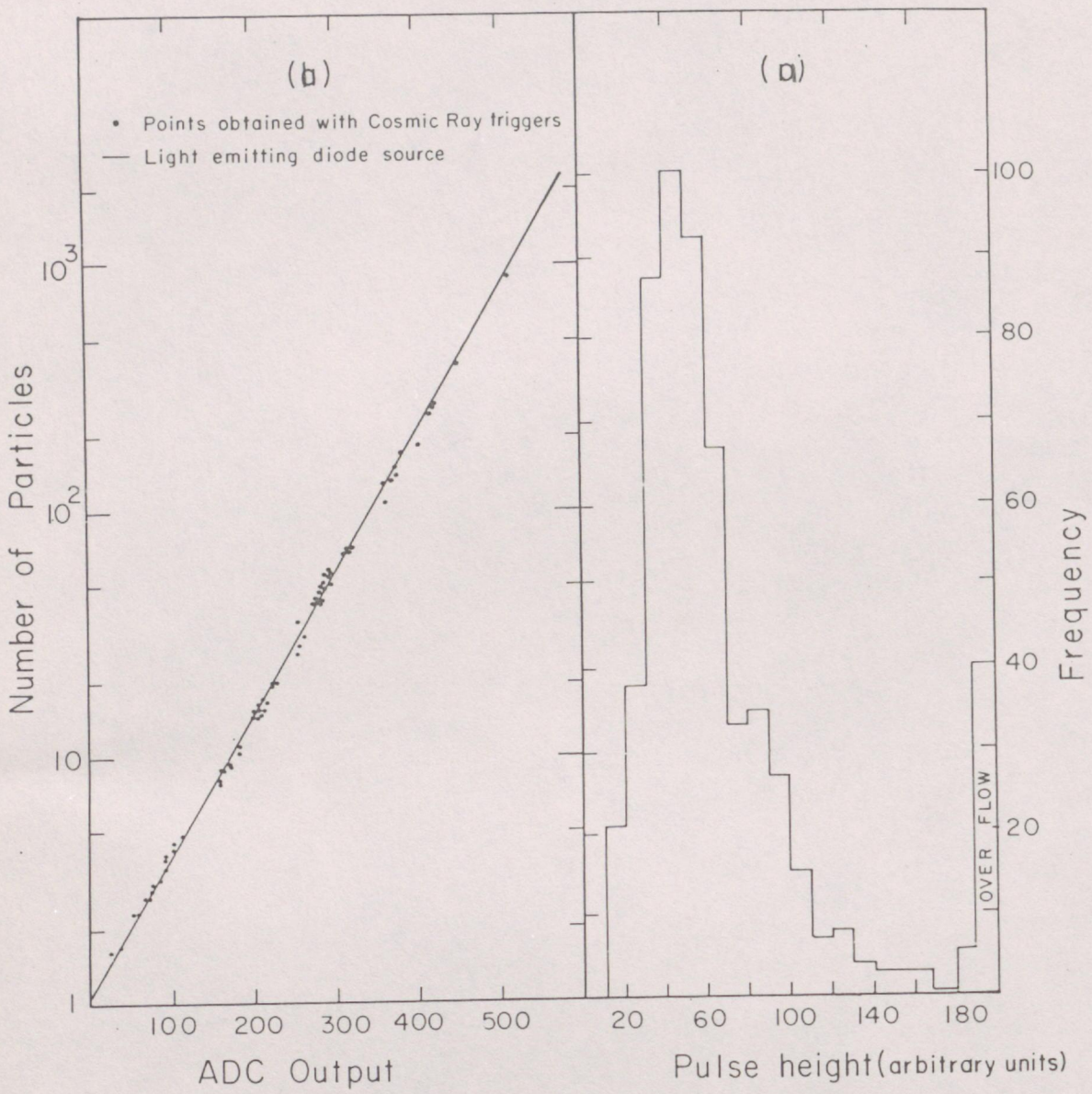

Figure 5.(a) Single particle response of a 2.25 m^2 density detector obtained with minimum ionising cosmic ray muons selected by a narrow angle GM counter telescope.

(b) A typical log-linear (LL) calibration for one of the 2.25 m^2 density detectors.

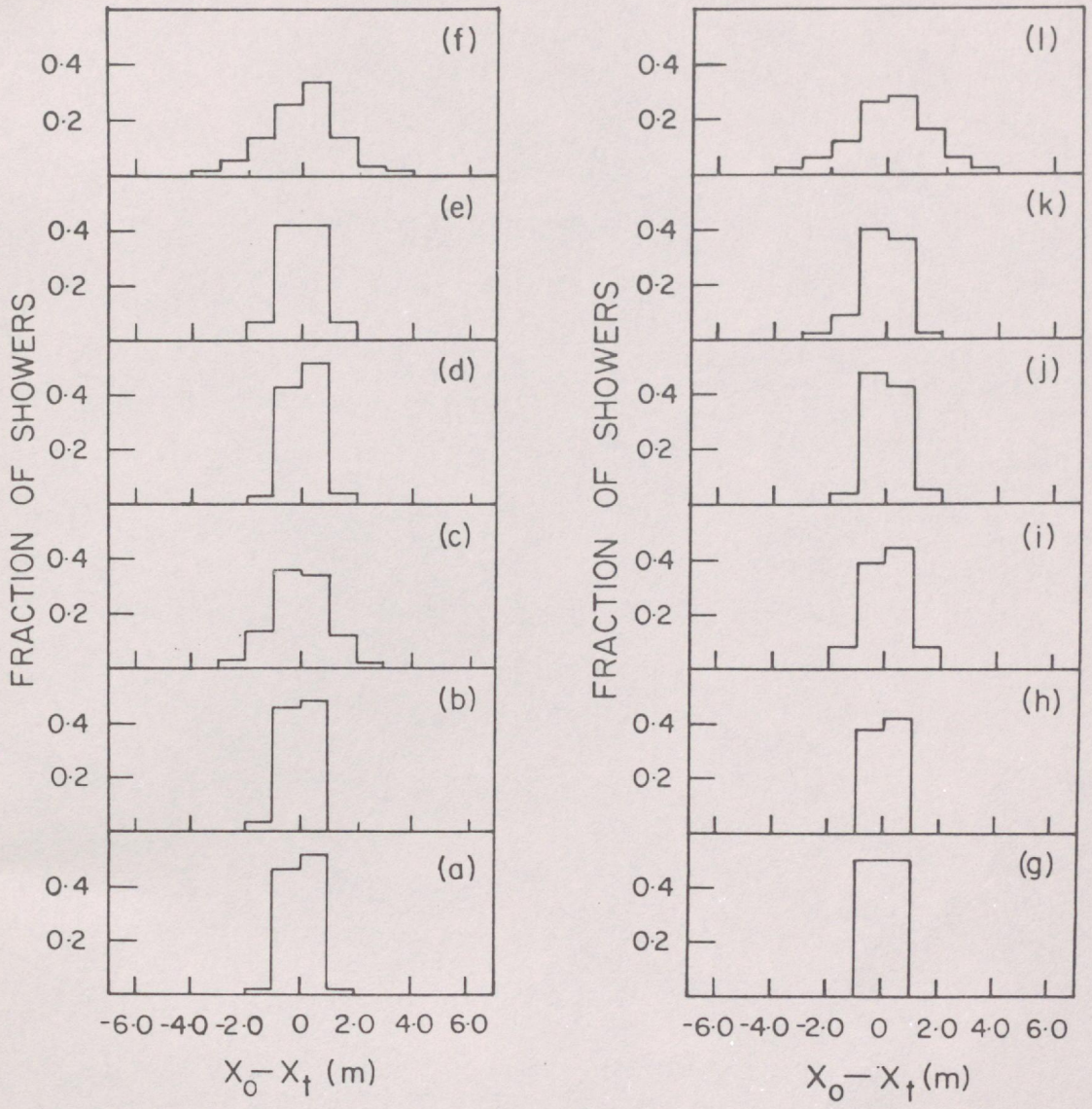

Figure 6.Distribution of deviations in core location ($x_o - x_t$), due to the fitting procedure, for some typical values of the true parameters.

(a) to (f) : $N_t = 10^4$ and (g) to (l) : $N_t = 8 \times 10^4$
(a), (b) and (c) : $r_1 = 0$ m and $r_2 = 5$ m.
(d), (e) and (f) : $r_1 = 10$ m and $r_2 = 15$ m.
(g), (h) and (i) : $r_1 = 5$ m and $r_2 = 10$ m.
(j), (k) and (l) : $r_1 = 15$ m and $r_2 = 20$ m.
(a), (d), (g) and (j) : $s_t = 0.6$
(b), (e), (h) and (k) : $s_t = 1.0$
(c), (f), (i) and (l) : $s_t = 1.4$

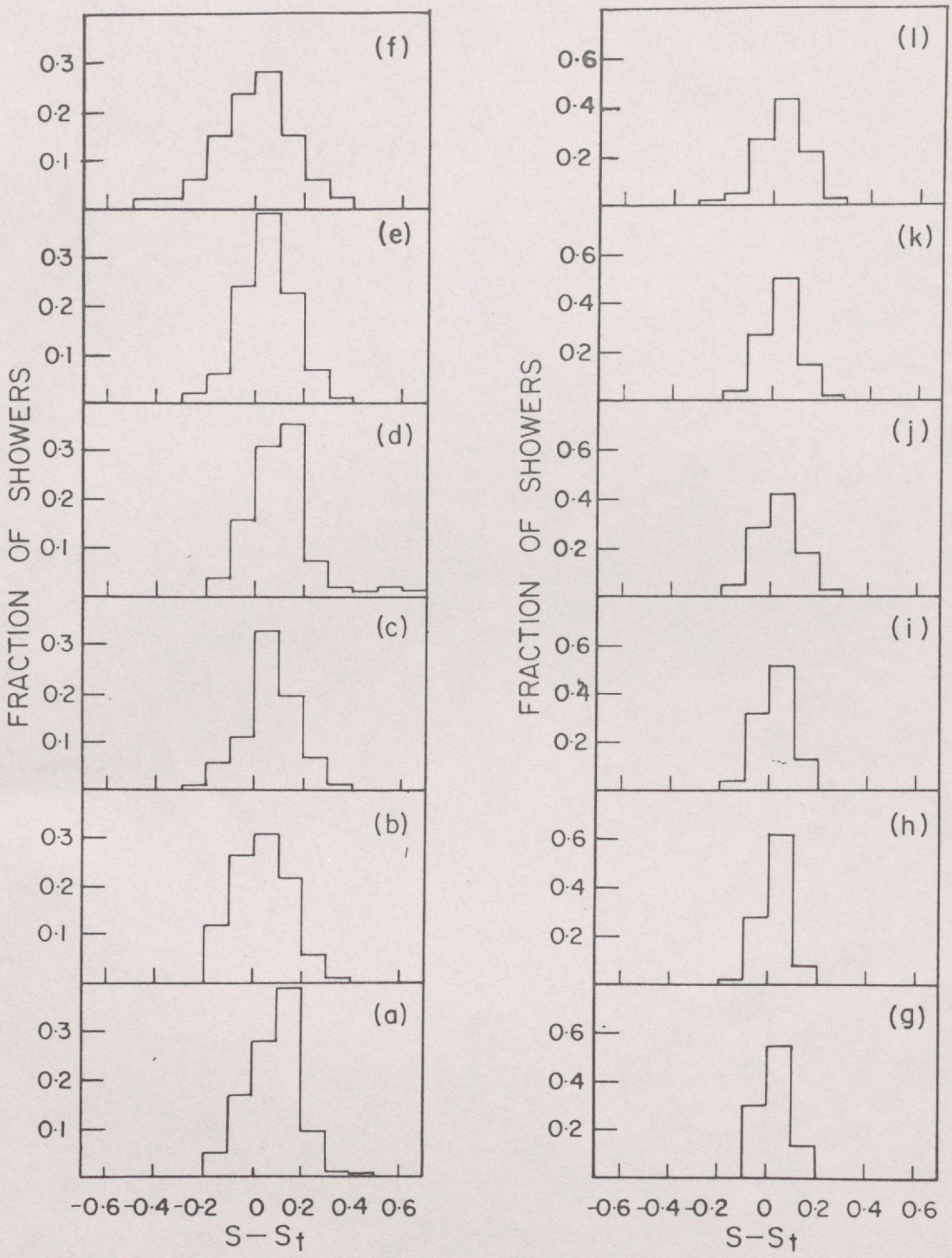

Figure 7. Distribution of deviations in the age parameter ($s_o - s_t$), due to the fitting procedure, for some typical values of the true parameters. Explanations for the symbols are the same as in figure 6.

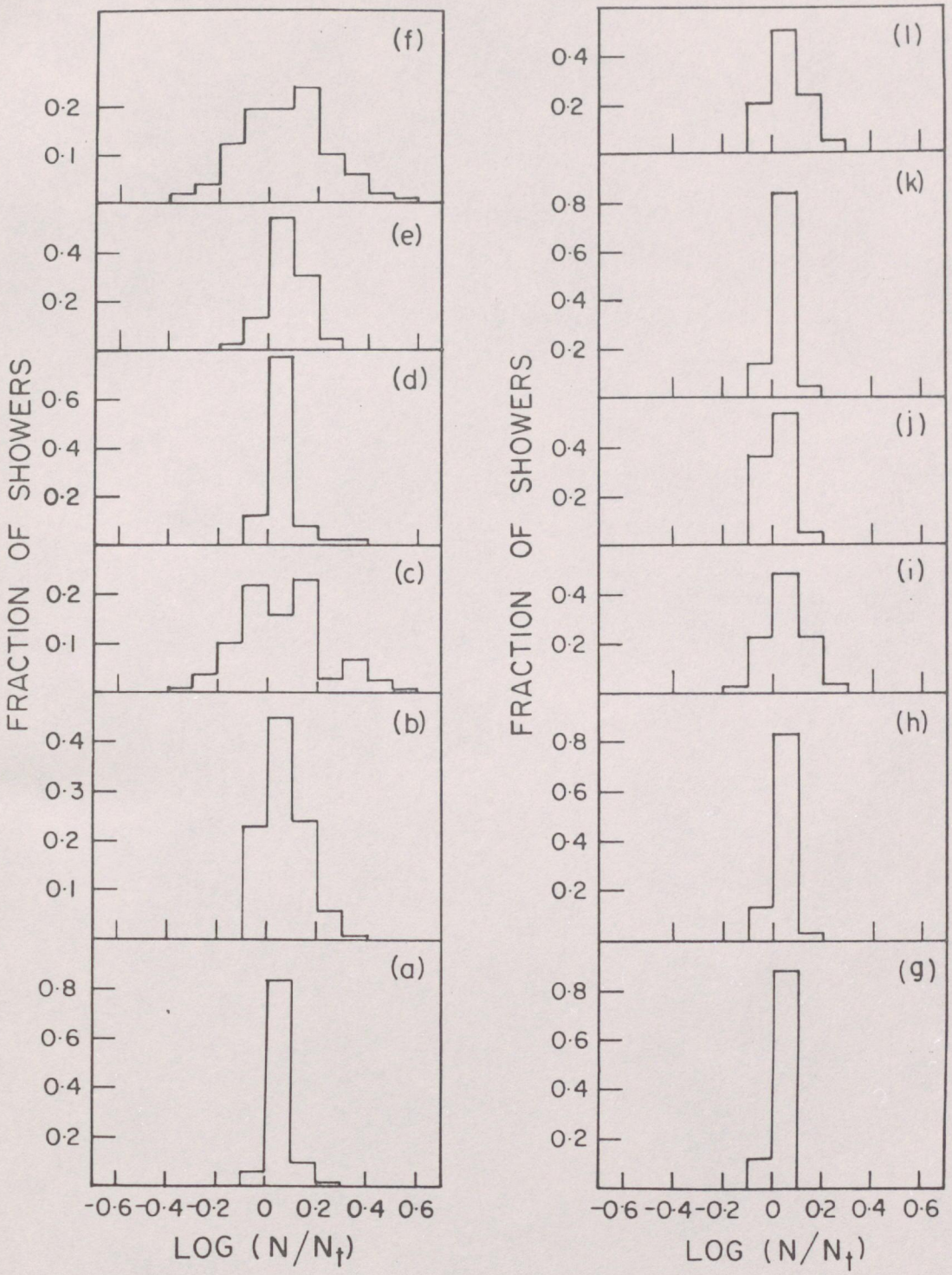

Figure 8. Distribution of deviations in shower size ($\log(N/N_t)$), due to the fitting procedure, for some typical values of the true parameters. Explanations for the symbols are the same as in figure 6.

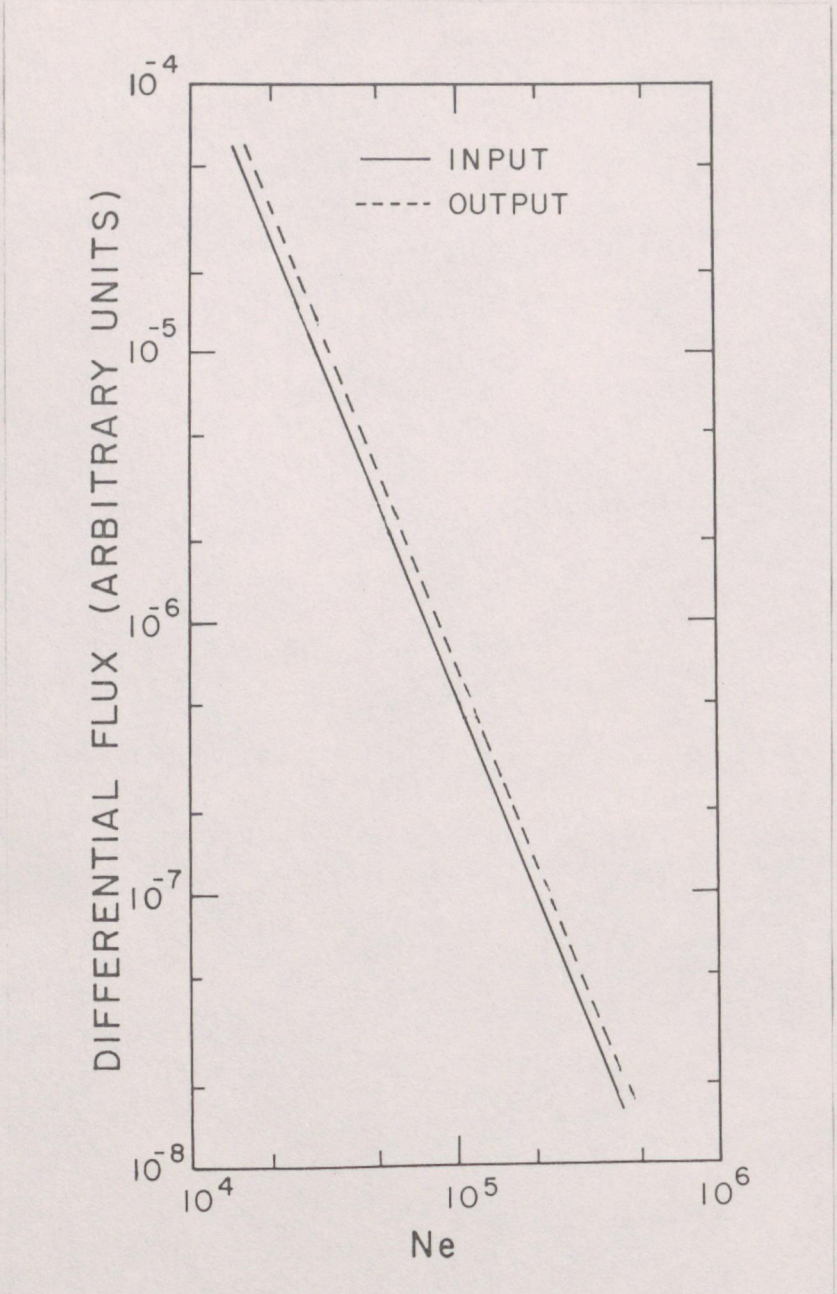

Figure 9.The assumed (continuous line) and the estimated (dashed line) size spectra from the shower analysis procedure.

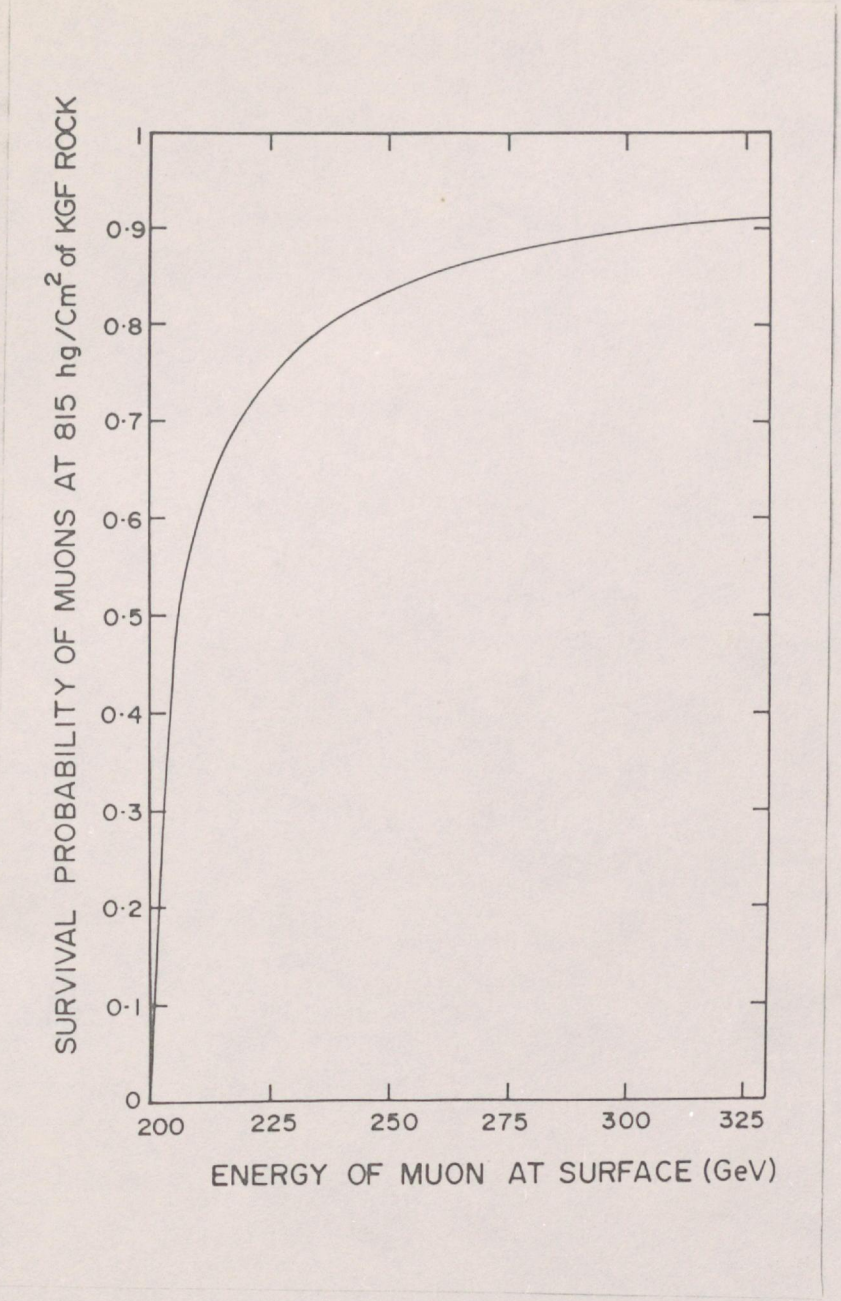

Figure 10. The survival probability at a depth of 815 hg cm^{-2} of Kolar rock as a function of the energy of the muon on the surface.

Nuclear Instruments and Methods in Physics Research A270 (1988) 556–571
North-Holland, Amsterdam

EXTENSIVE AIR SHOWER EXPERIMENT AT KOLAR GOLD FIELDS

B.S. ACHARYA, S. NARANAN, M.V.S. RAO, K. SIVAPRASAD, B.V. SREEKANTAN and SRIKANTHA RAO *

Tata Institute of Fundamental Research, Bombay 400005, India

Received 16 December 1987

An experiment to determine the nature of primary cosmic rays of energy $>10^{14}$ eV by studying high energy (> 220 GeV) muons and their correlations with other parameters of extensive air showers generated by them, was carried out at Kolar Gold Fields, India (atmospheric depth of 920 g cm^{-2}). An accurate estimate of shower parameters in showers as small as 10^4 particles was achieved by means of a closely packed array of large area detectors and by employing special methods of analysis. In this paper, the details of the array, the data recording system, the procedure of data analysis and error estimates are described.

1. Introduction

The study of ultrahigh energy ($> 10^{14}$ eV) cosmic rays is important to gain knowledge regarding their origin as well as features of high energy interactions in an energy region inaccessible to accelerators. Investigation of extensive air showers (EAS) generated by these cosmic rays is the only means at present because of low fluxes. The features of EAS generally depend on the characteristics of high energy interactions as well as on the nature of the primary particles. Of the various components of EAS, the high energy muon component carries information regarding these two aspects rather directly because of its origin in the first few generations of the EAS cascade [1]. We have earlier reported results on the gross features of high energy muons, in particular the variation of their number with shower size and their energy spectrum [2–4]. Interpretation of even such relatively direct information in terms of either the nature of the primary particles or features of high energy interactions uniquely, is difficult because of its sensitivity to both these aspects. The situation is even worse with regard to other EAS parameters, e.g. hadrons, low energy muons etc. Special methods have to be developed in order to disentangle the effects due to these two aspects on EAS parameters; e.g. study of correlations among properly chosen parameters.

We have shown [5,6] that a study of correlations between the density of low energy (> 1 GeV) and high energy (> 220 GeV) muons in showers of $\sim 10^4$ particles (primary energy $\sim 10^{14}$ eV) can yield unambiguous information regarding the nature of the primary particles. The negative correlation between the density of low energy muons at a fixed distance from the core and the number of high energy muons beyond a certain critical distance, in showers initiated by primaries of the same mass, can be exploited to discern between a primary cosmic ray composition that is "mixed" and one that is dominated by a single species. The correlation between the age parameter of the shower and the distance at which the high energy muon is detected can be similarly exploited.

An important feature of cosmic rays to be studied from the point of view of their origin is their energy spectrum. Direct measurements with detectors flown in satellites [7] have shown that the all particle integral energy spectrum (the spectrum of all species combined together) follows a power law with an exponent of -1.7 up to 10^{15} eV without any change in the exponent. Beyond this energy, the spectrum has been derived from EAS studies and the exponent in this energy region is about -2.1, suggesting that the primary energy spectrum becomes steeper at around a few times 10^{15} eV, thus forming the famous "knee". There are very few measurements from the EAS experiments below the knee to conclusively show that the knee is real. Models of the cosmic ray origin and propagation predict the primary cosmic ray composition to vary with energy in the neighbourhood of the knee, if it is real, in specific ways. Thus, it is essential to measure the the energy spectrum and the composition over a wide energy range including the knee.

We have carried out an experiment at Kolar Gold Fields (KGF, atmospheric depth: 920 g cm^{-2}) to elucidate all these aspects. The experiment is designed to provide accurate information on the size spectrum

* Now with the National Radio and Electronics Co. Ltd., Bombay 400 058, India.

(the dependence of the intensity of cosmic rays on size, the total number of particles contained in the showers generated by them) and the variation of the total number of muons of energy > 220 GeV with shower size over the size range 10^4 to 10^7, which covers the knee region, the lateral distribution of these muons and their correlations with low energy muons and the age parameter in the lower energy region. The array consists of a large number of scintillation detectors to accurately measure the electron component, a low energy (> 1 GeV) muon detector and a neon flash tube telescope and scintillators located underground to measure muons of energy > 220 GeV.

An accurate estimate of shower parameters at sizes as small as 10^4 particles was achieved by deploying closely spaced large area detectors up to 20 m from the center of the array. A computerised recording system and an on-line calibration procedure was used to handle the large number of detectors. Particular attention was paid to the analysis of showers with small sizes to obtain their parameters accurately. In section 2, the design of the EAS array and the various detectors used to measure the different shower parameters are described. The various triggers used to collect the data, the recording system and the calibration of the detectors are described in section 3. The method of analysis used to estimate the shower parameters and their errors is described in section 4.

2. Experimental setup

The extensive air shower array was specifically designed to detect and accurately measure showers as small as 10^4 particles as well as to collect enough showers of 10^7 particles. This was achieved by placing a large number of closely packed large area detectors at the center of the array and extending the array up to 100 m from the center.

The experimental setup consisted of an array of 70 plastic scintillation detectors (density detectors) to detect the showers and to measure the shower particle densities, five fast liquid scintillation detectors to measure the arrival direction of the showers, a shielded plastic scintillation detector (low energy muon detector) of 9 m^2 area to measure muons of energy > 1 GeV and four plastic scintillators (high energy muon detectors) located 270 m underground, vertically below the EAS

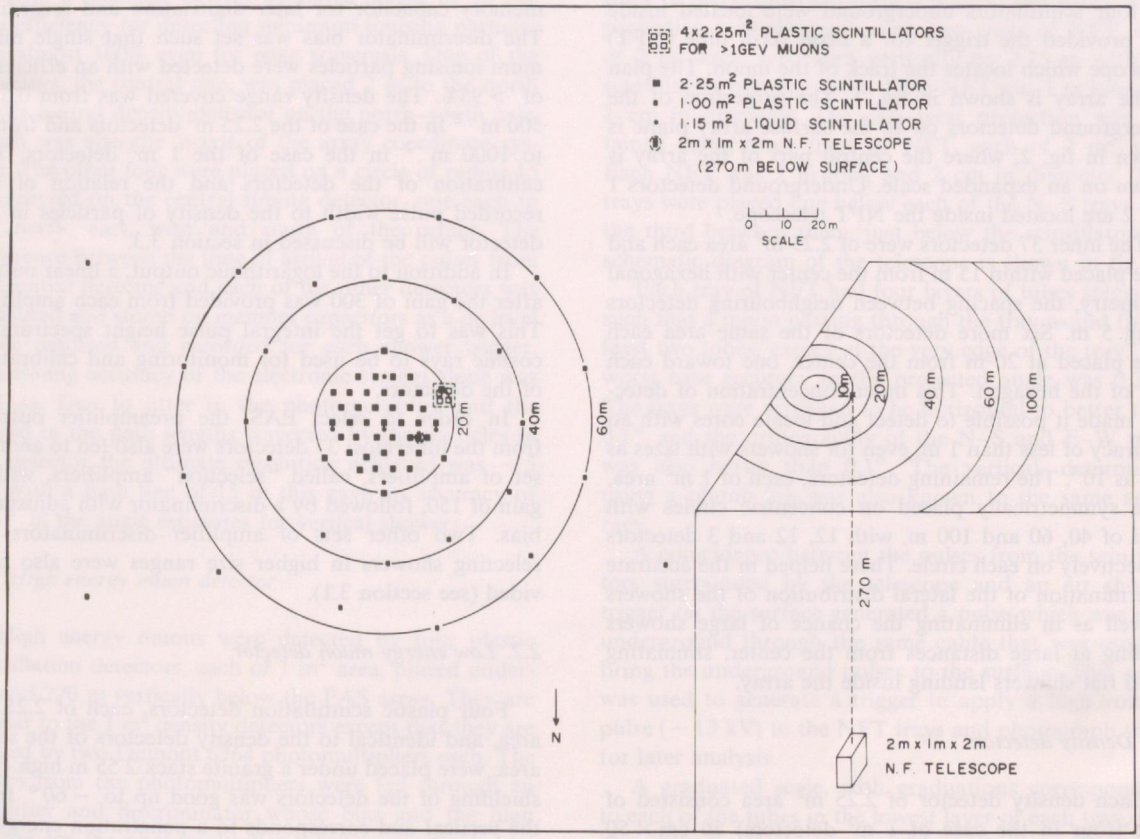

Fig. 1. The extensive air shower array at Kolar Gold Fields. The inset shows the location of the underground NFT telescope with respect to the surface array.

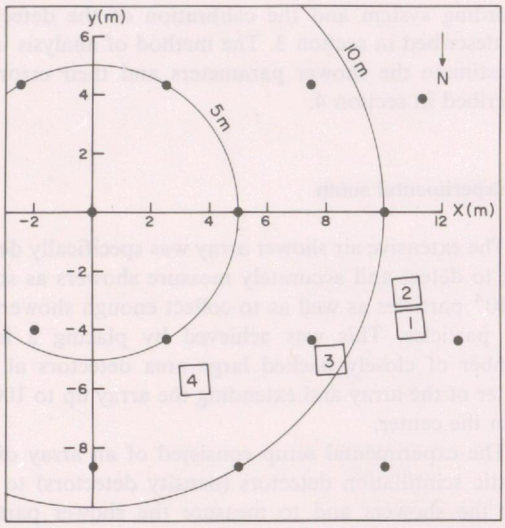

Fig. 2. Expanded view of the central region of the EAS array showing the positions of the underground detectors projected onto the plane of the surface array. Underground detectors 1 and 2 are located inside the NFT telescope.

array to measure muons of energy > 220 GeV; two of the four scintillators underground were located inside and provided the trigger for a neon flash tube (NFT) telescope which locates the track of the muon. The plan of the array is shown in fig. 1. The projection of the underground detectors on to the surface array plane is shown in fig. 2, where the central part of the array is shown on an expanded scale. Underground detectors 1 and 2 are located inside the NFT telescope.

The inner 37 detectors were of 2.25 m^2 area each and were placed within 15 m from the center with hexagonal symmetry, the spacing between neighbouring detectors being 5 m. Six more detectors of the same area each were placed at 20 m from the center, one toward each side of the hexagon. This inner concentration of detectors made it possible to detect and locate cores with an accuracy of less than 1 m, even for showers with sizes as low as 10^4. The remaining detectors, each of 1 m^2 area, were symmetrically placed on concentric circles with radii of 40, 60 and 100 m, with 12, 12 and 3 detectors respectively on each circle. These helped in the accurate determination of the lateral distribution of the showers as well as in eliminating the chance of large showers landing at large distances from the center, simulating small flat showers landing inside the array.

2.1. Density detectors

Each density detector of 2.25 m^2 area consisted of nine (four in the case of 1 m^2 detectors) 50 cm $\times$ 50 cm $\times$ 5 cm plastic scintillator blocks viewed by a Dumont 6364 photomultiplier (cathode diameter 12.7 cm) from a height of 80 cm, all the elements held in a light tight pyramidal aluminum container. The walls and the base of the pyramid were coated inside with TiO_2 paint for good light reflection. The light emitted by the scintillator, when ionising particles passed through it, was thus diffused before reaching the photocathode. Pulses from the photomultiplier were amplified by a high input impedance preamplifier [8] of gain 10 and transmitted to a central recording room by RG-11/U coaxial cable. Here the pulses were further amplified by a non-overloading amplifier by a factor of ~ 300, preserving the decay time of the pulses [8]. The decay time of the pulses from each detector was kept approximately at 5 μs by adjusting the anode resistance of the photomultiplier and the input capacitance of the preamplifier. The rise time of the pulses at the output of the 300 gain amplifiers varied from 100 to 500 ns, depending on the detector. The 300 gain amplifier was followed by a discriminator with an adjustable bias. As the decay time of the pulse was preserved, the width of the discriminator output was proportional to the logarithm of the height of the input pulse. Whenever certain trigger requirements were fulfilled (see section 3.1) the discriminator output was gated to a ramp followed by a stretching circuit where the ramp height was stored on a memory capacitor for later digitisation and recording. The discriminator bias was set such that single minimum ionising particles were detected with an efficiency of $> 95\%$. The density range covered was from 0.5 to 500 m^{-2} in the case of the 2.25 m^2 detectors and from 1 to 1000 m^{-2} in the case of the 1 m^2 detectors. The calibration of the detectors and the relation of the recorded pulse width to the density of particles in the detector will be discussed in section 3.3.

In addition to the logarithmic output, a linear output after the gain of 300 was provided from each amplifier. This was to get the integral pulse height spectrum of cosmic rays to be used for monitoring and calibration of the detectors.

In order to select EAS, the preamplifier outputs from the innermost 37 detectors were also fed to another set of amplifiers, called "selection" amplifiers, with a gain of 150, followed by a discriminator with adjustable bias. Two other sets of amplifier–discriminators for selecting showers in higher size ranges were also provided (see section 3.1).

2.2. Low energy muon detector

Four plastic scintillation detectors, each of 2.25 m^2 area, and identical to the density detectors of the same area, were placed under a granite stack 2.55 m high. The shielding of the detectors was good up to $\sim 60°$ from the vertical and corresponds to a penetration energy of 1 GeV for vertical muons. With a density of 3.02 g cm^{-3}, Z/A of 0.5 and Z^2/A of 6.3, the shielding

provided nearly 30 radiation lengths or 10 nuclear interaction lengths of matter for absorbing the soft component and hadrons. Pulse processing and recording of information from these scintillators were identical to that of the density detectors.

2.3. Energy flow detectors

Two plastic scintillators of 1 m^2 area each were placed one below the other with 2.5 cm of lead between them. The relative pulse heights in the two detectors gave a measure of the energy flow in the soft component. Pulse processing, monitoring, calibration and data recording were identical to the density detectors. This pair of detectors was placed 6 m from the center of the array.

2.4. Fast timing detectors

These were five liquid scintillation detectors, each of 1 m^2 area, and viewed by a fast RCA 6810 (or Philips 56 AVP) photomultiplier. The liquid used was commercial grade Shellsol-A with paraterphenyl and POPOP as solutes. The detector had a cylindrical (pill box) geometry with a diameter of 1.15 m and a height of 30 cm. The efficiency for detecting minimum ionising particles was almost 100% even for edge traversals. One of the detectors, the central one, was placed 2 m to the north of the central density detector on the north–south axis, which was also the y-axis of the array coordinate system. The other four were placed on a circle of radius 15 m centered on the central timing detector, one each to the north, east, west and south of the center. The difference between the time of arrival of the pulses from the central detector and each of the other detectors was measured and stored on memory capacitors as a dc level to be digitised and recorded for each shower trigger. The timing accuracy of the electronic system alone was ~ 2 ns. Due to jitter in the photomultiplier and the spread in the path lengths traversed by the particles in the detector the ultimate resolution achieved was ~ 5 ns. With a base line of 15 m this gave an accuracy of $\sim 5°$ in the angle estimates for vertical showers.

2.5. High energy muon detector

High energy muons were detected by four plastic scintillation detectors, each of 1 m^2 area, placed underground 270 m vertically below the EAS array. They are similar to the 1 m^2 density detectors except that they are viewed by two Dumont 6364 photomultipliers each. The pulses from the photomultipliers were fed through an amplifier and discriminator whose bias and the high voltage for the photomultiplier tubes were adjusted so that minimum ionising particles were detected with an efficiency $> 95\%$ by each photomultiplier. At an ambient temperature of $\sim 32°C$ this led to a large rate ($\sim$ a few thousand per minute) of pulses from a single photomultiplier, almost all due to dark current and some due to background radioactivity. In order to avoid a large number of accidental associations with the shower trigger on the surface, a twofold coincidence between the discriminator outputs belonging to the same detector was taken, reducing the detector output rate to 50–150 pulses per minute. Most of these were due to local radioactivity. The chance association rate with EAS triggers was thus reduced to approximately 7.5% of the recorded rate of such associations. The twofold output from each detector was delayed, using HH-4000 delay cable, by an amount characteristic of the detector (varying from 2 to 10 μs) and mixed with the undelayed pulse. Pairs of pulses from all the four detectors were further mixed and sent to the recording room on the surface by an RG-11/U cable. On the surface the pulses were time-sorted and pulses from individual detectors were tagged and stored to record the yes/no information in the event of a trigger.

Two of the scintillators were surrounded by a neon flash tube (NFT) telescope to locate the muon track. Crossed NFT trays were used to get projections of the track in two orthogonal vertical planes. The north–south projection was obtained using two trays of NFT, each of 2 m^2 area, separated vertically by 2.25 m with the scintillators between them. Each NFT was 1 m long and 1 cm in diameter. The east–west projection was obtained using three trays of NFT, each of 2 m^2 area. Each NFT was 2 m long and 2 cm in diameter. Two trays were placed one below each of the N–S trays and the third between them, just below the scintillators. A schematic diagram of the telescope is shown in fig. 3.

Each tray of NFT had four layers of tubes staggered such that a muon passing through the tray would fire at least two tubes, except at the very edge of the tray. The worst case accuracy in the projected angle was 0.25°. The trays were arranged to be horizontal to better than 0.1° and the orthogonally of the N–S and E–W trays was also better than 0.1°. The vertical, determined using a plumb line,was also known to the same accuracy.

A coincidence between the pulses from the scintillators surrounded by the telescope and an air shower trigger on the surface generated a pulse which was sent underground through the same cable that was used to bring the underground pulses to the surface. This pulse was used to generate a trigger to apply a high voltage pulse (~ 13 kV) to the NFT trays and photograph them for later analysis.

A graduated scale, with graduations corresponding to each of the tubes in the lowest layer of each tray, was illuminated and photographed in each event. The scale was placed just below each tray so that for each event the serial number of each tube that had flashed in the

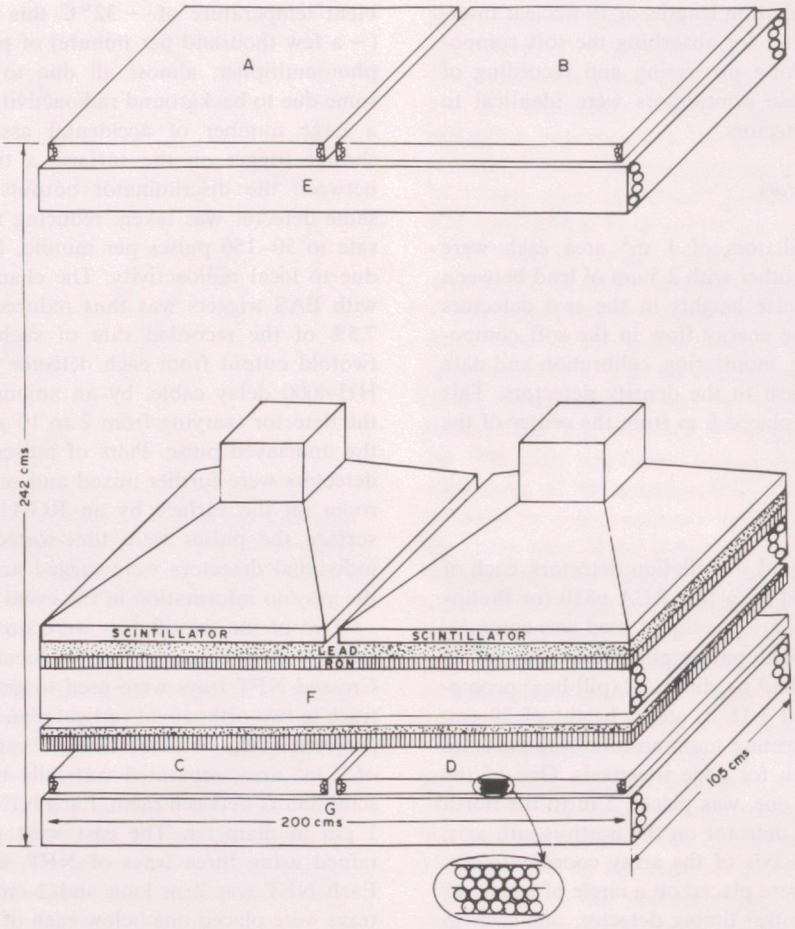

Fig. 3. Schematic view of the underground neon flash tube telescope. The staggering of the NFT tubes is also shown in the expanded view.

lowest layer was known. Knowing the pattern of tubes in each tray, the serial numbers of tubes that flashed in the other layers were also easily obtained. A system of mirrors was used to photograph both the projected tracks on the same frame of the film. The delay between the passage of the muon through the telescope and the application of the high voltage pulse to the flash tubes was $\sim 10\ \mu s$ (which includes the muon travel time from surface to the underground detectors and the cable delay for the pulses from the underground detectors to travel to the surface laboratory and the trigger pulse to travel from the surface to the underground laboratory), sufficiently small to operate the tubes with an efficiency of $\sim 85\%$. With four layers of tubes per tray, the track location efficiency was 96%.

3. Data recording

In order to collect an adequate number of showers of small size, the triggering system was designed to yield a large area of collection for these showers. This resulted in a high triggering rate and hence a large relative dead time. Thus, it became necessary to operate the array with different triggering systems at different times for showers of different sizes. Moreover, a separate triggering system had to be adopted for collecting showers with a high energy muon in the underground detector because of the small number of these muons per shower. The various triggers employed to record the data are described below.

3.1. Types of triggers

3.1.1. S (surface) trigger

Air showers were selected by a threefold coincidence between any set of three adjacent detectors forming an equilateral triangle of side 5 m, among the innermost 37 detectors, with at least three particles in each of them (for part of the runs only the innermost 19 detectors were used for this selection). This trigger selected

showers of 10^4 particles with good efficiency up to 15 m from the center. Though the rate of these triggers was ~ 30 per minute, the actual rate of recording was ~ 5 per minute because of a dead time of 10 s (see section 3.2). In all, about 35 000 such triggers were recorded during 120 h of operation. Most of the showers collected with this trigger were in the size range 5×10^3 to 10^5. No other trigger was on when this trigger was operating.

3.1.2. SD and LS triggers

The SD and LS (large size) triggers were used to collect showers of medium and large size respectively. Since the rate of these two triggers was low, dead time effects were minimum. The SD trigger required 10 particles in the central detector and 6 particles in each of three symmetrically placed detectors in the 5 m ring. The size threshold for efficient triggering in this case was 4×10^4 and the trigger rate was 80 per hour. The LS trigger required 15 particles in each of three symmetrically placed detectors in the 20 m ring giving a size threshold of 1.6×10^5 particles and a trigger rate of 10 per hour.

In all, about 30 000 SD showers and about 35 000 LS showers were collected during 400 and 3000 h respectively.

3.1.3. SU trigger

Showers associated with high energy muons were selected by a coincidence of the S-trigger pulse and any of the pulses from the underground muon detectors (U pulses). A 6 μs resolving time was used for this coincidence to accommodate the transit time of the muons from the surface to the underground level as well as the pulse transit time through the cable. The rate of U pulses was approximately 600 per minute, which gave rise to SU coincidences purely by chance at the rate of < 0.2 per hour. The observed rate of SU coincidences was ~ 3 per hour. A subset of SU showers, called SUT showers, had at least one muon passing through the

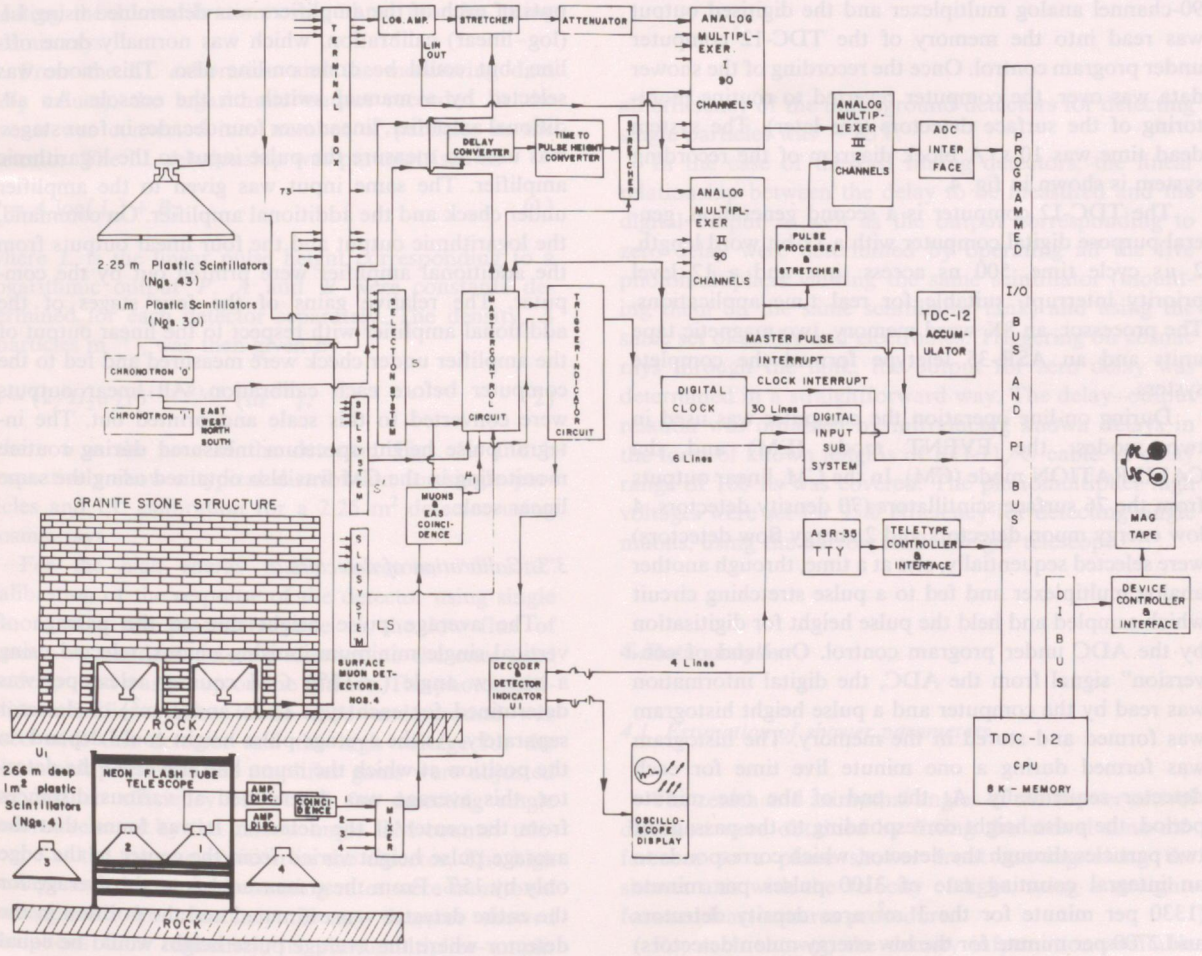

Fig. 4. Block diagram of the computerised recording and monitoring system.

telescope. In all, about 30000 SU showers were recorded in 10000 h of operation, out of which about 3000 were SUT showers in which the muon track was unambiguously defined with tracks in all the five NFT trays.

The LS and SU triggers were run concurrently because of their low rates, whereas the S and SD showers were collected in separate runs.

3.2. Recording system and calibration procedures

Any of the triggers outlined above initiated the recording of the shower information. The density information from all the detectors, the fast timing information, the yes/no information from the underground detectors, the date and time of arrival of the shower, information regarding non-working detectors and some housekeeping information were all recorded on magnetic tape using a TDC-12 on-line computer [9]. The logarithmic output from each detector, available as analog dc level on memory capacitors, was sequentially fed to a 12-bit analog to digital converter (ADC) through a 90-channel analog multiplexer and the digitised output was read into the memory of the TDC-12 computer under program control. Once the recording of the shower data was over, the computer reverted to routine monitoring of the surface detectors (see later). The system dead time was 10 s. A block diagram of the recording system is shown in fig. 4.

The TDC-12 computer is a second generation, general purpose digital computer with a 12-bit word length, 2 μs cycle time, 500 ns access time and a 12 level priority interrupt, suitable for real time applications. The processor, an 8K word memory, two magnetic tape units and an ASR-35 teletype formed the complete system.

During on-line operation the computer was used in two modes, the EVENT mode (EM) and the CALIBRATION mode (CM). In the CM, linear outputs from the 76 surface scintillators (70 density detectors, 4 low energy muon detectors and 2 energy flow detectors) were selected sequentially, one at a time, through another analog multiplexer and fed to a pulse stretching circuit which sampled and held the pulse height for digitisation by the ADC under program control. On "end of conversion" signal from the ADC, the digital information was read by the computer and a pulse height histogram was formed and stored in the memory. The histogram was formed during a one minute live time for each detector sequentially. At the end of the one minute period, the pulse height corresponding to the passage of two particles through the detector, which corresponds to an integral counting rate of 3100 pulses per minute (1330 per minute for the 1 m^2 area density detectors and 2700 per minute for the low energy muon detectors) was estimated by interpolation. The interpolation accuracy was 20 mV, the ADC accuracy. The interpolated pulse height for the current period along with that of the previous sampling and a message, if these two differed by more than 20%, were all printed out and the computer switched to monitoring the next detector. The current values of the interpolated pulse heights for all the detectors were always resident in the memory. These were fed into the memory before the start of the run and were continuously updated in the CM. The monitoring of each detector was, thus, carried out every 1.5 h assessing its performance. This monitoring routine formed the background program for on-line operation, with the EVENT interrupt given top priority. The occurrence of any trigger mentioned earlier was termed an EVENT. When an EVENT occurred the monitoring was suspended, the data pertaining to the EVENT recorded and the program reverted back to resume monitoring from where it was suspended due to the EVENT interrupt. A crystal clock oscillator provided clock signals every 100 ms to the computer for time keeping.

The relation between the logarithmic and linear outputs of each of the amplifiers was determined using LL (log–linear) calibration, which was normally done off-line, but could be done on-line also. This mode was selected by a manual switch on the console. An additional amplifier, linear over four decades in four stages, was used to measure the pulse input to the logarithmic amplifier. The same input was given to the amplifier under check and the additional amplifier. On command, the logarithmic output and the four linear outputs from the additional amplifier were printed out by the computer. The relative gains of the four stages of the additional amplifier with respect to the linear output of the amplifier under check were measured and fed to the computer before each calibration. All linear outputs were converted to this scale and printed out. The integral pulse height spectrum measured during routine monitoring in the CM was also obtained using the same linear scale.

3.3. Calibration of detectors

The average pulse height due to the passage of vertical single minimum ionising muons, selected using a narrow angle ($< 12°$) GM counter telescope, was determined for each type (2.25 and 1 m^2) of detector separately. As the average pulse height could depend on the position at which the muon had traversed the detector, this average was determined at various distances from the center of the detector. It was found that the average pulse height varied from the center to the edge only by 15%. From these measurements, the average for the entire detector was estimated and the position in the detector where the average pulse height would be equal to the detector average was determined. The mean of

the pulse height distribution, obtained with the narrow angle telescope, at this average position was then determined with good accuracy ($< 1\%$) and was thereafter used as the response of the detector for vertical single particles. All distributions were truncated at twice the peak value for determining the averages.

The density spectrum, i.e. the integral pulse height distribution, for the omnidirectional cosmic rays passing through the detector, was then determined up to 100 particles. This spectrum could be well approximated by a power law of slope -3.0. The rate of pulses above the two particle pulse height, H_2 (equal to twice the average single muon pulse height), was obtained from this spectrum and was thereafter used for monitoring the detector. The level of two particles was chosen as the optimum to keep the noise contribution to a minimum and to obtain a reasonably accurate density spectrum in that region during one minute of monitoring time.

The LL calibration was done, for all detectors, at the beginning of the experiment using a light emitting diode to cover a dynamic range of four decades. The constancy of the log–linear relation was checked by repeating the LL calibration every three months, using cosmic rays.

From the LL calibration and the monitoring data (H_2 values), the logarithmic output recorded in the events was converted into number of particles in the detector. The LL relationship was parametrised as

$$P = A \log(L) + B, \qquad (1)$$

where L is the linear pulse height corresponding to a logarithmic output P. A and B were constants determined for each detector separately. The density, Δ (particles m^{-2}), was then given by

$$\Delta = (2/H_2 a)10^{(P-B)/A}\ (m^{-2}), \qquad (2)$$

where a is the area of the detector. Figs. 5a and b respectively show a typical distribution for single particles and LL calibration for a 2.25 m^2 detector using cosmic rays.

For the high energy muon detectors, "in situ" calibration of the response of the detector using single muons was not practicable due to the low flux of muons. A standard detector identical to the ones used underground was set up on the surface. The photomultiplier–amplifier system to be used underground was used with this detector and the high voltage for the photomultipliers and the amplifier gains were adjusted to yield an efficiency of $> 90\%$ for detecting single muons, selected by the narrow angle GM counter telescope at the average position in the detector. The high voltage and the twofold counting rates were monitored underground for constancy. If any detector showed deviations from constancy, its photomultiplier–amplifier system was brought up for recalibration. The overall efficiency of the underground detectors for detecting single particles was $\sim 85\%$.

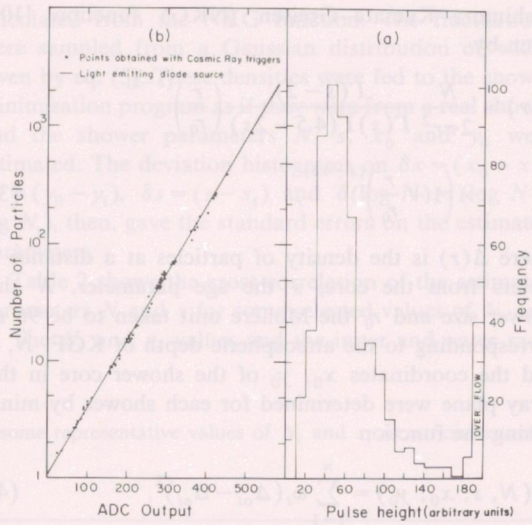

Fig. 5. (a) Single particle response of a 2.25 m^2 density detector obtained with minimum ionising cosmic ray muons selected by a narrow angle GM counter telescope. (b) A typical log–linear (LL) calibration for one of the 2.25 m^2 density detectors.

In the case of the fast timing detectors, the linear relationship between the delay to be measured and the digital output as well as the output corresponding to zero delay were determined by operating all the five photomultipliers viewing the same scintillator (mounting them on the same scintillator tank) and using the same set of cables and electronics. Triggering on cosmic rays through the tank, the output for zero delay was determined in a straightforward way. The delay–output relation was obtained by introducing known delays in the form of known lengths of RG-11/U cable. A delay range of 100 ns was covered. The photomultiplier high voltages were set for 95% efficiency for detecting single muons, using the narrow angle Geiger telescope.

4. Data analysis

4.1. Estimation of shower parameters

The zenith and azimuthal angles of the shower arrival direction were obtained by fitting the arrival time differences to a plane shower front moving along the shower axis with the velocity of light, using a straightforward least-squares procedure.

For each shower, the density information available in the distance range 2–60 m was fitted to the

Nishimura–Kamata–Greisen (NKG) function [10], given by

$$\Delta(r) = \frac{N}{2\pi r_0^2} \frac{\Gamma(s-2)}{\Gamma(s)\Gamma(4.5-2s)} \left(\frac{r}{r_0}\right)^{(s-2)} \times \left(1+\frac{r}{r_0}\right)^{(s-4.5)}, \quad (3)$$

where $\Delta(r)$ is the density of particles at a distance r meters from the core, s the age parameter, N the shower size and r_0 the Molière unit taken to be 96 m corresponding to the atmospheric depth of KGF. N, s and the coordinates x_0, y_0 of the shower core in the array plane were determined for each shower by minimising the function

$$\chi^2(N, s, x_0, y_0) = \sum_{i=1}^{n} \omega_i (\Delta_{oi} - \Delta_{ei})^2, \quad (4)$$

where

$$\omega_i = \sigma_i^{-2} = \left[a_i \Delta_{ei} + (0.2 a_i \Delta_{ei})^2\right]^{-1}, \quad (5)$$

using the method of steepest descent, similar to the one used by the MIT group [11]. Here Δ_{oi} and Δ_{ei} are the observed and expected (according to the NKG function) densities and a_i and ω_i are the area and the weight factor for the ith detector respectively. The first term in eq. (5) corresponds to the statistical error and the second one to the systematic error, which is estimated to be 20%. For computational convenience, only the first term was included for densities less than $25/a_i$ and only the second one beyond, as these terms dominate in the corresponding regions. The minimisation was carried out on the CDC 3600 computer system at the Tata Institute of Fundamental Research, using a FORTRAN program developed for the purpose.

An important feature of the present experiment is the accuracy with which parameters of showers with sizes as low as 10^4 particles have been obtained. At these sizes the density of particles expected beyond a few meters from the core, where the bulk of the data was available, was only a few particles per m^2. So a large number of detectors record no particles due to fluctuations that carry the observed density below threshold. If these "zero density" detectors are ignored during analysis, an unduly flat lateral distribution would be obtained for the shower as only those detectors which showed an upward fluctuation would be used. However, if the number of detectors with near-threshold densities was small, using them in the analysis would have steepened the distribution in a large fraction of the showers, the fraction depending on the smallest expected density. In the present experiment a fairly large number (~ 25) of detectors with near-threshold densities were available for showers of about 10^4 particles and therefore we could use the "zero density" detectors for analysis and estimate the parameters accurately even for very low sizes. The accuracy of the estimated parameters at these low sizes has been determined using artificial showers, analysed using the same procedure as for the real showers, to be described in section 4.3.

Table 1
The different types of triggers and information obtained from them

Trigger	Information obtained	Size range
S, SD&LS	(1) Size spectrum	10^4–10^7
	(2) Age distribution	10^4–10^7
	(3) Low energy muon density	10^4–10^7
S&SUT	(1) Lateral distribution and total number of muons of energy > 220 GeV	10^4–3.2×10^5
SUT	(1) Low energy muon density	10^4–3.2×10^5
	(2) Correlation between low energy muon density and the distance of the high energy muon	
S, SD, LS&SU	(1) Total number of high energy muons	10^4–10^7

4.2. Classification of showers

All the data have been primarily classified according to the estimated size. Table 1 summarises the several aspects on which information has been obtained from the present experiment. Since showers are classified according to size, the migration of showers from one size group to the other, due to errors in the analysis, has to be carefully taken into account. This has been done using the analysis of artificial showers.

4.3. Estimation of errors

The iterative minimisation procedure described earlier does not lend itself easily to a determination of the errors in the estimated parameters. An easier and more straightforward way, for this purpose, is the use of "artificial showers". An "artificial shower" is a set of "observed" densities in the detectors of the EAS array, constructed from the NKG distribution and the estimated fluctuations, with the shower parameters (size N_t, age s_t and coordinates of the core x_t, y_t) assumed "a priori". Estimating the shower parameters using this set of densities by the iterative procedure gave an estimate of the deviations of the estimated parameters from the true ones.

The artificial showers were generated using the Monte Carlo method. Because of the circular symmetry of the array, the errors on the estimated parameters are ex-

pected to be dependent only on the distance of the shower core from the center of the array and not on the actual core location. The array was, therefore, divided into a number of annular rings around the array center, each of 5 m width, up to a distance of 20 m – the distance up to which most of the real showers were accepted for final analysis. Showers were allowed to fall uniformly in each ring. For each set of values of N_t and s_t, 400 showers were generated in each annular ring. For each shower, a set of "observed" densities in all the detectors were generated by imposing fluctuations, using the Monte Carlo technique, on the average densities calculated from the NKG function. The fluctuations were sampled from a Gaussian distribution of width given by eq. (5). These densities were fed to the shower minimisation program as if they were from a real shower and the shower parameters N, s, x_0 and y_0 were estimated. The deviation histograms on $\delta x = (x_0 - x_t)$, $\delta y = (y_0 - y_t)$, $\delta s = (s - s_t)$ and $\delta(\log N) = (\log N - \log N_t)$, then, gave the standard errors on the estimated parameters.

Table 2 shows the cross-correlation of the estimated parameters N and s for some selected values of N_t and s_t. The N_t and s_t values and the inner and outer radii

Table 2
Percentage of showers with different estimated values of N and s for some representative values of N_t and s_t in various annular rings of radii r_1 and r_2
Table 2(a)

$s \rightarrow$	0.4	0.5	0.6	0.7	0.8	0.9	1.0	1.1	1.2	1.3	1.4	0.5	0.6	0.7	0.8	0.9	1.0	1.1	1.2	1.3	1.4
$\text{Log}(N/10^4)$ ↓	$N_t=10^4$ $s_t=0.6$ $r_1=0\text{m}$; $r_2=5\text{m}$											$N_t=10^4$ $s_t=0.6$ $r_1=10\text{m}$; $r_2=15\text{m}$									
0.5	–	–	–	–	–	–	–	–	–	–		–	–	–	–	–	–	–	–	0.5	–
0.4	–	–	–	–	–	–	–	–	–	–		–	–	–	–	–	–	–	0.8	0.8	–
0.3	–	–	–	–	–	0.3	0.3	–	–	–		–	–	–	–	–	–	0.5	1.0	–	–
0.2	0.5	–	–	1.8	6.5	0.5	0.3	–	–	–		1.0	1.0	0.5	1.8	0.8	1.5	0.5	–	–	–
0.1	4.0	16.0	25.0	36.0	3.0	0.3	–	–	–	–		2.8	13.0	26.5	28.0	6.3	0.5	–	–	–	–
0.0	0.3	1.0	3.0	2.0	–	–	–	–	–	–		–	1.8	4.3	5.8	0.3	–	–	–	–	–
−0.1	$N_t=8\cdot10^4$ $s_t=0.6$ $r_1=5\text{m}$; $r_2=10\text{m}$											$N_t=8\cdot10^4$ $s_t=0.6$ $r_1=15\text{m}$; $r_2=20\text{m}$									
1.1	–	–	–	–	–	–	–	–	–	–		3.0	2.3	–	–	–	–	–	–	–	–
1.0	0.5	29.0	47.8	10.8	–	–	–	–	–	–		1.3	23.3	22.5	5.0	0.5	–	–	–	–	–
0.9	–	1.5	7.5	2.5	0.3	–	–	–	–	–		0.3	1.3	18.5	12.8	2.3	0.5	–	–	–	–
0.8	–	–	–	–	–	–	–	–	–	–		–	–	–	–	0.5	–	–	–	–	–
0.7	$N_t=10^4$ $s_t=1.0$ $r_1=0\text{m}$; $r_2=5\text{m}$											$N_t=10^4$ $s_t=1.0$ $r_1=10\text{m}$; $r_2=15\text{m}$									
0.3	–	–	–	–	–	–	–	–	–	0.5		–	–	–	–	–	–	–	–	0.3	0.5
0.2	–	–	–	–	–	–	–	1.8	4.0	–		–	–	–	–	–	–	–	0.5	3.0	0.3
0.1	–	–	–	–	–	–	4.8	17.3	2.0	–		–	–	–	–	–	0.8	9.5	16.0	3.3	–
0.0	–	–	–	–	1.0	16.0	25.6	2.8	–	–		–	–	–	–	2.3	16.3	28.0	6.0	–	–
−0.1	–	–	–	0.3	11.3	10.8	1.0	–	–	–		–	–	–	1.3	3.5	6.5	1.3	–	–	–
−0.2	–	–	–	–	–	–	–	–	–	–		–	–	0.3	0.8	–	–	–	–	–	–
	$N_t=8\cdot10^4$ $s_t=1.0$ $r_1=5\text{m}$; $r_2=10\text{m}$											$N_t=8\cdot10^4$ $s_t=1.0$ $r_1=15\text{m}$; $r_2=20\text{m}$									
1.1	–	–	–	–	–	–	–	3.0	0.3	–		–	–	–	–	0.3	0.8	1.5	1.3	0.3	0.3
1.0	–	–	–	–	0.3	17.3	60.3	5.3	–	–		–	–	–	0.8	3.3	20.5	42.8	13.3	1.8	0.3
0.9	–	–	–	–	1.3	10.8	1.8	–	–	–		–	–	–	–	0.5	6.0	6.0	0.8	–	–
0.8																					

Table 2(b)

$N_t = 10^4$, $s_t = 1.4$, $r_1 = 0$m; $r_2 = 5$m

Log(N/10^4) ↓ \ s →	0.8	0.9	1.0	1.1	1.2	1.3	1.4	1.5	1.6	1.7	1.8
0.7	–	–	–	–	–	–	–	–	–	0.3	
0.6	–	–	–	–	–	–	–	–	–	0.8	
0.5	–	–	–	–	–	–	–	–	2.8	–	
0.4	–	–	–	–	–	–	–	3.5	3.5	–	
0.3	–	–	–	–	–	–	1.5	12.0	0.3	–	
0.2	–	–	–	–	–	–	17.5	4.8	–	–	
0.1	–	–	–	–	–	3.3	13.3	–	–	–	
0.0	–	–	–	–	5.5	15.8	0.3	–	–	–	
−0.1	–	–	–	3.0	4.8	2.5	–	–	–	–	
−0.2	–	–	0.8	2.5	0.5	–	–	–	–	–	
−0.3	0.3	–	0.5	0.3	–	–	–	–	–	–	
−0.4											

$N_t = 10^4$, $s_t = 1.4$, $r_1 = 10$m; $r_2 = 15$m

Log(N/10^4) ↓ \ s →	0.9	1.0	1.1	1.2	1.3	1.4	1.5	1.6	1.7	1.8
0.7	–	–	–	–	–	–	–	–	–	–
0.6	–	–	–	–	–	–	–	–	–	1.0
0.5	–	–	–	–	–	–	–	–	0.8	0.8
0.4	–	–	–	–	–	–	–	2.3	3.8	0.3
0.3	–	–	–	–	–	–	1.3	7.3	1.3	–
0.2	–	–	–	–	–	2.0	16.0	5.5	–	–
0.1	–	0.3	–	–	0.3	9.0	9.5	–	–	–
0.0	–	0.3	–	0.3	6.0	11.5	0.8	–	–	–
−0.1	–	0.3	0.3	3.3	7.5	1.0	–	–	–	–
−0.2	–	–	0.8	1.5	1.3	–	–	–	–	–
−0.3	–	1.3	0.5	0.3	–	–	–	–	–	–
−0.4										

$N_t = 8 \cdot 10^4$, $s_t = 1.4$, $r_1 = 5$m; $r_2 = 10$m

Log(N/10^4) ↓ \ s →	0.8	0.9	1.0	1.1	1.2	1.3	1.4	1.5	1.6	1.7	1.8
1.4	–	–	–	–	–	–	–	–	–	–	
1.3	–	–	–	–	–	–	–	–	–	–	
1.2	–	–	–	–	–	–	–	3.5	0.3	–	
1.1	–	–	–	–	–	–	13.0	9.8	–	–	
1.0	–	–	–	–	–	12.5	36.0	–	–	–	
0.9	–	–	–	–	1.8	19.0	1.5	–	–	–	
0.8	–	–	–	0.3	2.3	0.3	–	–	–	–	
0.7											

$N_t = 8 \cdot 10^4$, $s_t = 1.4$, $r_1 = 15$m; $r_2 = 20$m

Log(N/10^4) ↓ \ s →	0.9	1.0	1.1	1.2	1.3	1.4	1.5	1.6	1.7	1.8
1.4	–	–	–	–	–	–	–	–	–	0.3
1.3	–	–	–	–	–	–	–	0.3	–	–
1.2	–	–	–	–	–	–	–	3.0	2.0	–
1.1	–	–	–	–	–	0.3	9.3	14.3	0.5	–
1.0	–	–	–	–	0.8	14.0	31.0	4.0	–	–
0.9	–	–	0.3	1.3	4.0	11.8	2.3	0.3	–	–
0.8	–	–	–	–	0.3	0.5	–	–	–	–
0.7										

(r_1 and r_2 respectively) of the annular ring within which the cores are selected are also shown in the table. The numbers given in the main body of the table are the percentage of showers in each bin of N and s. It can be seen that there is a general trend of N being overestimated when s is overestimated and vice versa, particularly for the smallest and the flattest showers, as expected. However, the fraction of such showers is not very large, and for larger and steeper showers this effect is quite small. Figs. 6, 7 and 8 respectively show the δx, δs and $\delta(\log N)$ distributions for the same group of showers as in table 2. The sample standard deviations σ_x, σ_y, σ_s and $\sigma_{\log N}$ for these showers are shown in table 3. It can be seen that σ_x and σ_y are less than a meter and $\sigma_s < 0.15$ in most of the cases.

4.4. Triggering efficiency of the array

The triggering criteria discussed in section 3.1 set the threshold for showers to be recorded by the recording system. For further analysis, additional software selection criteria were imposed at the time of analysis. The criterion was size dependent and required a sevenfold (four-fold for showers in the estimated size between 2×10^4 and 4×10^4) coincidence of detectors forming

Table 3
Rms deviations of the estimated parameters from the true ones

N_t	s_t	r_1 [m]	r_2 [m]	σ_x [m]	σ_y [m]	$\sigma_{\log N}$	σ_s
10^4	0.6	0	5	0.38	0.38	0.028	0.11
10^4	1.0	0	5	0.51	0.45	0.081	0.11
10^4	1.4	0	5	1.05	1.07	0.170	0.14
10^4	0.6	10	15	0.47	0.55	0.066	0.14
10^4	1.0	10	15	0.74	0.71	0.075	0.12
10^4	1.4	10	15	1.50	1.50	0.170	0.17
8×10^4	0.6	5	10	0.26	0.26	0.018	0.06
8×10^4	1.0	5	10	0.36	0.37	0.035	0.06
8×10^4	1.4	5	10	0.75	0.65	0.078	0.07
8×10^4	0.6	15	20	0.66	0.66	0.060	0.09
8×10^4	1.0	15	20	0.87	0.86	0.030	0.08
8×10^4	1.4	15	20	1.60	1.50	0.080	0.09

The integrals in eq. (9) are dependent on the geometry of the array, the selection criteria (through ϵ) and the errors in the estimation of shower parameters (through G). As the evaluation of the function G over the entire parameter space and subsequent integration takes a lot of computer time the integrals are replaced by summations and evaluated using the Monte Carlo method. As before, showers were allowed to be incident uniformly over an area, A_t, covering the range of x_t and y_t and extending up to a distance r_m from the center of the array where $\epsilon \leq 1\%$, densities in the triggering detectors calculated, fluctuations imposed. Showers satisfying the selection criteria were analysed as if they were real showers and the parameters N, s, x_0, y_0 were estimated. The range of N_t covered, from 2.5×10^3 to 6.4×10^5, was divided into 48 equal logarithmic intervals and the range of 0.4 to 1.8 in s was covered in 28 bins of width 0.05 each. For computational convenience, only four values of r_m – 20, 50, 100 and 150 m corresponding to the size intervals $(0.25–1) \times 10^4$, $(1–4) \times 10^4$, $(0.4–1.6) \times 10^5$ and $(1.6–6.4) \times 10^5$ respectively – were used. Showers whose estimated cores were within the area, $A(N, s)$ (see table 5), were then used for calculating $p(N_t, s_t, N, s)$. If $n(N_t, s_t, N, s)$ were the number of showers so picked (usually 20) with size N and age s out of $n_g(N_t, s_t, N, s)$ showers generated over an area $A_t(=\pi r_m^2)$ with size N_t and age s_t, then

$$p(N_t, s_t, N, s) = n(N_t, s_t, N, s) A_t / n_g(N_t, s_t). \tag{10}$$

Substituting this into eq. (8), $f_{obs}(N)$ can be estimated from a given $f_t(N_t, s_t)$. Fig. 9 shows the input and output size spectra for an input spectrum, $f_t(N_t, s_t) \propto N_t^{-2.4}$. It is seen that the estimated fluxes are somewhat overestimated while the exponent remains the same. This has to be taken into account when the spectrum predicted by theory is compared with the experimental data.

For any other parameter, $g(N, s)$, of the showers we can generalise eq. (8) and estimate the expected average value of the parameter as

$$g_{exp}(N, s) = \frac{\int_{N_t}\int_{s_t} g(N_t, s_t) f_t(N_t, s_t) p(N_t, s_t, N, s)\, dN_t\, ds_t}{\int_{N_t}\int_{s_t} f_t(N_t, s_t) p(N_t, s_t, N, s)\, dN_t\, ds_t}. \tag{11}$$

An example of such a parameter studied in this experiment is the number of muons of energy > 220 GeV [12,13].

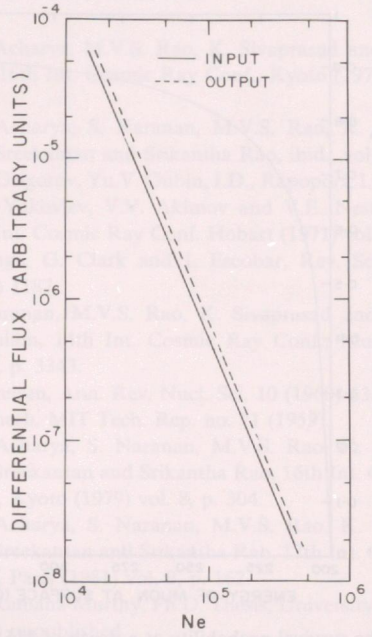

Fig. 9. The assumed (continuous line) and the estimated (dashed line) size spectra from the shower analysis procedure.

4.6. Analysis of the high energy muon data

Data on high energy muons were provided by the four scintillators and the neon flash tube telescope located 270 m underground. The overburden of rock above these detectors corresponds to 815 hg cm^{-2} of Kolar rock, which is essentially made of Hornblende schist and has a mean density of 3.02 g cm^{-3}, $\langle Z/A \rangle = 0.495$ and $\langle Z^2/A \rangle = 6.31$ [14]. The minimum energy required for a muon to reach this depth depends upon the energy loss. Though fluctuations in the energy loss are not very important at this depth, Krishnaswamy [15] calculated the survival probability of muons as a function of energy taking them into account. Fig. 10 shows this plot. Integrating the product of the survival probability and the differential energy spectrum of muons in air showers, taken to be $\propto E^{-2.5}$, gave the number of muons arriving at that depth. The energy at which the integral number of muons is equal to this number is the effective threshold energy and is estimated to be 220 GeV.

The determination of the lateral distribution of muons requires the measurement of the distance of the muon from the core. The core location is determined from the shower parameter analysis to an accuracy of 1 m in the region of the array where the shower detection efficiency is $> 90\%$ (see table 3). The location of the muon in the array coordinate system is given by the NFT data. From the known positions of the flashed tubes in the various layers in the NFT telescope, the

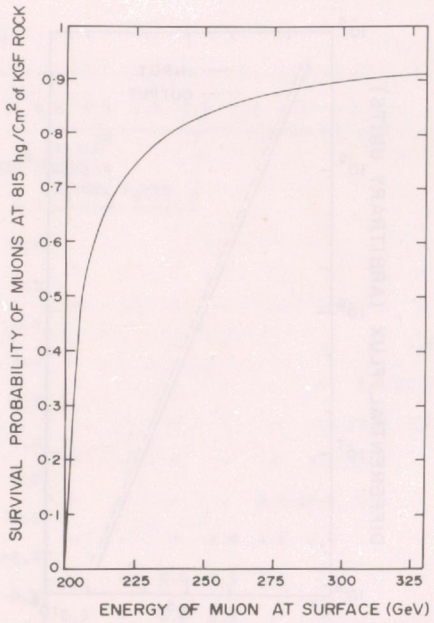

Fig. 10. The survival probability at a depth of 815 hg cm^{-2} of Kolar rock as a function of the energy of the muon on the surface.

projected trajectories of the muon in the two orthogonal planes were obtained. The muon trajectory in space, its point of intersection with the array plane and the distance of the muon from the core in the shower plane, assuming the muon arrival direction and the shower arrival direction are the same (since the energy of the muon is large the two directions are the same within a fraction of a degree – the angle between the two is $\sim p_t/E$, where p_t is ~ 0.3 GeV/c) were then calculated in a straightforward way.

The various sources of error in the determination of the distance of the muon from the shower core are the error due to the finite size of the NFTs and the geometry of the telescope, multiple Coulomb scattering of the muon in the rock above the underground telescope, the core location errors and finally the deflection of the muons in the geomagnetic field. The last source has to be taken into account, if it is large, when one compares the experimental lateral distribution with theoretical predictions which do not take this deflection into account. These errors have been estimated by Srikantha Rao [16] and are briefly discussed here.

Because of the finite diameter of the NFTs, several trajectories are possible for a given configuration of the tubes in the various trays. However, the error in the projected angles is small since the diameter of the tubes is small (1 and 2 cm), the tubes in each tray are staggered and the top and bottom trays in each view are separated by 2.25 m and it is estimated to be 0.1°. The error in the projected angles due to multiple Coulomb scattering is estimated to be 0.17° taking into account the energy loss of the muons in the rock and the energy spectrum of muons in air showers. The corresponding error in the location of the muon (in x and y) in the surface array plane due to the combined error in the projected angles is 0.9 m. This, combined with an error of 1 m in the core location (see table 3), results in an error of 1.9 m in the core distance of the muon in the shower plane. The deflection of the muons in the geomagnetic field is estimated to be 1.2 m taking into account their energy spectrum. The effective error for purposes of comparing the experimental data on the lateral distribution of muons with theoretical predictions which do not take the magnetic deflection into account is, therefore, 2.2 m. It should be noted that this error is independent of the core muon distance since the error in core location is nearly constant over the area where showers are accepted for final analysis (efficiency $> 90\%$) and the error in the muon location is also nearly independent of the zenith angle at least up to 20° (corresponding to a core muon distance of ~ 100 m), the maximum recorded angle in the data.

5. Conclusions

The extensive air shower array along with an underground neon flash tube telescope to detect muons of energy > 220 GeV, operated at Kolar Gold Fields, India, is described. The computerised recording system and the detector monitoring and calibration procedures are discussed in detail. The procedure of analysis for obtaining the shower parameters and the distance of the high energy muon from the shower core is described. An important feature of the experiment is the closely packed central region of the array, where large area detectors were deployed at a mutual separation of 5 m and within which small showers were accepted for final analysis, and the availability of a large number of density measurements near the threshold density. This feature enabled the parameters to be estimated accurately for sizes as small as 10^4 particles. The typical errors for the finally accepted showers are 1 m in the core location, 30% in shower size, 0.1 in the age parameter and 2.2 m in the core–muon distance.

Acknowledgements

We thank the management and staff of the Bharat Gold Mines Limited for the excellent facilities and cooperation extended by them, without which the experiment could not have been carried out. Messrs. P.B. Subramaniam and A.M. Gurumurthy installed and maintained the computer system and the interface electronics. Mr. A.V. John developed the complete software

for the on-line recording and monitoring system and several utility programs. Messrs. M.A. Patil, S.G. Khairatkar, A.D. Ranpura, S.D. Samuel and other staff members contributed extensively in the design and maintenance of all the detectors and the associated electronics. Dr. V.S. Narasimham and Messrs. H.D. Salvekar and R.M. Wankar helped in the construction of the NFT telescope. We thank all of them for their contributions.

References

[1] B.V. Sreekantan, Proc. Int. Cosmic Ray Conf., Jaipur (1963) vol. 4, p. 143.
[2] B.K. Chatterjee, S. Lal, T. Matano, G.T. Murthy, S. Naranan, K. Sivaprasad, B.V. Sreekantan, M.V.S. Rao and P.R. Vishwanath, Proc. Int. Cosmic Ray Conf., London (1965) vol. 2, p. 627.
[3] B.V. Sreekantan, Proc. 12th Int. Cosmic Ray Conf. Hobart (1971) vol. 7, p. 2706.
[4] S. Naranan, K. Sivaprasad, B.V. Sreekantan and M.V.S. Rao, Proc. 13th Int. Cosmic Ray Conf., Denver (1973) vol. 3, p. 1872.
[5] B.S. Acharya, M.V.S. Rao, K. Sivaprasad and Srikantha Rao, 16th Int. Cosmic Ray Conf., Kyoto (1979) vol. 8, p. 312.
[6] B.S. Acharya, S. Naranan, M.V.S. Rao, K. Sivaprasad, B.V. Sreekantan and Srikantha Rao, ibid., vol. 13, p. 272.
[7] N.L. Grigorov, Yu.V. Gubin, I.D., Rapoport, I.A. Savenko, B.M. Yakovlev, V.V. Akimov and V.E. Nesterov, Proc. 12th Int. Cosmic Ray Conf. Hobart (1971) vol. 5, p. 1746.
[8] K. Suga, G. Clark and I. Escobar, Rev. Sci. Instr. 32 (1961) 1187.
[9] S. Naranan, M.V.S. Rao, K. Sivaprasad and P.B. Subramaniam, 14th Int. Cosmic Ray Conf., Munich (1975) vol. 9, p. 3343.
[10] K. Greisen, Ann. Rev. Nucl. Sci. 10 (1960) 63.
[11] F. Scherb, MIT Tech. Rep. no. 71 (1959).
[12] B.S. Acharya, S. Naranan, M.V.S. Rao, K. Sivaprasad, B.V. Sreekantan and Srikantha Rao, 16th Int. Cosmic Ray Conf., Kyoto (1979) vol. 8, p. 304.
[13] B.S. Acharya, S. Naranan, M.V.S. Rao, K. Sivaprasad, B.V. Sreekantan and Srikantha Rao, 17th Int. Cosmic Ray Conf., Paris (1981) vol. 9, p. 162.
[14] P.V. Ramana Murthy, Ph.D. Thesis, University of Bombay (1962) unpublished.
[15] M.R. Krishnaswamy, Ph.D. Thesis, University of Bombay (1981) unpublished.
[16] Srikantha Rao, Ph.D. Thesis, University of Bombay (1981) unpublished.